Life and death of slow-moving landslides

Pascal Lacroix[1] ✉, *Alexander L. Handwerger*[2,3] *and Grégory Bièvre*[1]

Abstract | In the most destructive and catastrophic landslide events, rocks, soil and fluids can travel at speeds approaching several tens of metres per second. However, many landslides, commonly referred to as slow-moving landslides, creep at rates ranging from millimetres to several metres per year and can persist for years to decades. Although slow-moving landslides rarely claim lives, they can cause major damage to infrastructure and sometimes fail catastrophically, transitioning into fast-moving landslides that can result in thousands of casualties. In addition, slow-moving landslides are highly erosive features that control the landscape morphology in many mountainous regions (such as the California Coast Ranges or the Apennines). The persistent and long-term motion of slow-moving landslides provides an exceptional opportunity to investigate landslide processes and mechanisms. In this Review, we examine the environmental conditions (such as geology, climate and tectonics) of slow-moving-landslide-prone regions, analyse the forcings (for example, precipitation and groundwater, earthquakes, river erosion, anthropogenic forcings and external material supply) that drive their motion and investigate the subsequent implications of the different forcings on landslide dynamics. We then discuss circumstances in which slow-moving landslides can accelerate rapidly, move large distances or even fail catastrophically. Finally, we provide new perspectives and challenges for future landslide research.

Landslides are major natural hazards that cause thousands of casualties each year[1]. Catastrophic landslide events are the consequence of the rapid collapse and downslope transport of soil, rock and fluids, and are often triggered by heavy rainfall[2], earthquakes[3] or anthropogenic activities[1]. The destructive force of catastrophic landslides makes it nearly impossible to measure their physical parameters (such as the landslide velocity, groundwater content, basal friction and material damage) in the field during failure. Consequently, constraining the mechanisms that control slope failure remains challenging. Although it is difficult to monitor catastrophic landslides in real time, non-catastrophic, slow-moving landslides, which move downslope for months to decades (or even centuries) at rates ranging from millimetres to several metres per year, provide an excellent opportunity to study landslide processes[4].

Slow-moving landslides rarely claim lives[5], but fast-moving (m s^{-1}) debris flows can initiate from within the slow-moving landslide mass and inundate large areas[6,7]. In addition, slow-moving landslides sometimes accelerate rapidly and fail catastrophically, causing widespread destruction and casualties[8–10]. In fact, slow ground motions (mm $year^{-1}$ to m $year^{-1}$) have often been identified, retrospectively, as precursory deformation signals before catastrophic landslides[8,10–14]. One of the best examples of a slow-moving landslide that failed catastrophically is the 1963 Vajont landslide, Italy. After three years of slow motion at rates of about 1 m $year^{-1}$, which was initiated by a dammed-lake impoundment, the landslide mass collapsed into the lake, creating a tsunami that claimed 1,900 victims[8]. Thus, landslide detection before catastrophic collapse is a primary goal of current research.

Aside from the potential for runaway acceleration, slow-moving landslides also permanently affect the lives of local communities by destroying human infrastructure[5,15–17] and agriculture[18]. As a consequence, local communities must adapt to live with landslides or migrate to new regions[19]. Furthermore, slow-moving landslides play a major role in controlling the evolution of mountainous landscapes and cause substantial erosion over geomorphic timescales[20,21].

Slow-moving landslides occur in large numbers across the world in areas that typically have mechanically weak, clay-rich soil and rock, and high seasonal precipitation. Slow-moving landslides exhibit non-uniform spatial and temporal kinematic changes[22–24] and tend to be deep-seated (>3 m thick)[21,25] with a complex subsurface hydrological system[26]. The term 'slow-moving landslides' has been used to describe a wide variety of landslide styles, including those that flow, creep, topple and slide.

[1]*Université Grenoble Alpes, Université Savoie Mont Blanc, CNRS, IRD, IFSTTAR, ISTerre, Grenoble, France.*

[2]*Joint Institute for Regional Earth System Science and Engineering, University of California, Los Angeles, Los Angeles, CA, USA.*

[3]*Jet Propulsion Laboratory, California Institute of Technology, Pasadena, CA, USA.*

✉*e-mail: pascal.lacroix@univ-grenoble-alpes.fr*

https://doi.org/10.1038/s43017-020-0072-8

Key points

- Slow-moving landslides occur all around the world in mechanically weak rock and soil.
- The persistent and long-term motion of slow-moving landslides provides an exceptional opportunity to investigate landslide processes and mechanisms.
- The landslide velocity is modulated by external forcings (such as precipitation, earthquakes, material supply and anthropogenic activity).
- Slow-moving landslides can sometimes accelerate rapidly and fail catastrophically.

Here, we specifically define slow-moving landslides as masses of coherent soil and rock that move, primarily by frictional sliding along discrete shear zones and/or by viscous flow, at rates ranging from a few mm year^{-1} to 100 m year^{-1} (defined by REF.[27] as very slow to intermediate velocity landslides). Therefore, our definition of slow-moving landslides uses a wider velocity range than previous definitions[27], incorporating a range of velocities that are measurable by modern ground-based and remote-sensing monitoring techniques. We also define the time period over which a slow-moving landslide remains active as its 'life' and the point at which it stops moving, often as a result of changes in stress due to erosion or catastrophic collapse, human engineering or long periods of drought, as its 'death'. While this terminology is not often used to describe landslides, we feel it provides context that allows us to differentiate slow-moving landslides from more commonly known catastrophic landslides.

The first mention of slow-moving landslides dates back to the early twentieth century[28], and their velocity was first measured in the 1930s, with pioneering work in the USA and New Zealand[29–31]. Since that time, several hundreds of slow-moving landslides have been monitored worldwide, with either geodetic or geophysical measurements. The main aim of slow-landslide monitoring is to evaluate the hazard posed by their motions and to understand their role in landscape evolution. It is impossible to refer to all studies of slow-moving landslides here, so, instead, we focus on a selection of landslides that have increased understanding of their physical properties. The landslides discussed are selected on the basis of several criteria, including the presence of long-term, multi-parameter monitoring (such as displacement, groundwater and seismicity analysis), coupled with a sufficient characterization of the landslide properties (for example, the geology, geometry, mechanism and velocity), environment and forcing factors (such as precipitation events, earthquakes, human activity and coastal or river erosion).

In this Review, we provide a synthesis of 80 years of research on slow-moving landslides. We focus on recent advances in data collection since the 1970s that have enabled continuous landslide monitoring via ground-based[23,32–39] and remote-sensing techniques[9,10,18,40–47] and, consequently, has facilitated a better understanding of landslide mechanics[25,32,33,48–51]. We examine the environmental conditions of landslide-prone regions, analyse the forcings that drive their motion, the subsequent implications on their mechanics (for example, their basal friction, bulk damage and chemical processes) and discuss circumstances where slow-moving landslides can accelerate rapidly or even fail catastrophically. Finally, we present new opportunities and challenges for future landslide research.

Environmental conditions

TABLE 1 presents the key characteristics of 31 well-known, slow-moving-landslide regions (FIG. 1), with landslide surface areas ranging between 0.03 and 2.5 km^2 (FIG. 2). FIGURE 1 reveals several clusters of reported landslides, which can partly be explained by the development of national landslide observatories over the past 20 years (OMIV[52], USGS-USA), and the cultural aspects of the landslide hazard mitigation: for example, in some parts of Italy, governments at the regional scale take charge of landslide monitoring[53]. More generally, the spatial distribution of reported slow-moving landslides emphasizes that detection and monitoring is usually only a concern in developed countries (for example, Western Europe[8,54–62], the USA[6,10,25,63–68], New Zealand[69–71] and Japan[72]). Several factors can explain the geographical distribution in monitoring of slow-moving landslides, such as poorly funded natural-hazard-management programmes and a priority to manage deadly catastrophic landslides at the local and national government level in less economically developed countries. However, monitoring of slow-moving landslides is taking place in some less economically developed countries (such as Peru, Congo and Iran), in part, owing to collaborations between developed and less economically developed countries[16,18,43,44,50,73].

Despite the geographical gaps in research on slow-moving landslides, the current inventory covers a wide variety of environmental and geological conditions (TABLE 1). Many mountain chains worldwide, such as the European Alps, Alborz, southern Alps of New Zealand, Apennines, Rockies, Andes, Japanese Alps, Virunga Mountains and California Coast Ranges (FIG. 1), which have major differences in seismicity (low to moderate seismicity in the French Alps, strong earthquakes in Japan, New Zealand or Peru), precipitation (several metres per year in the southern Alps of New Zealand, desertic areas — as low as 2 cm year^{-1} — in the western margin of the Peruvian Andes), elevation (near sea level in the California Coast Ranges to thousands of metres high in the Rockies) and rock type (accretionary prism mélange in the California Coast Ranges; gneiss in the Italian Alps; volcanic/lacustrine rocks in Peru; shales in Japan; flysch in the northern Apennines, Italy), are affected by slow-moving landslides.

Most slow-moving landslides typically occur in weak materials, either Quaternary soils or highly damaged sedimentary layers with gentle slope angles (<20°; FIG. 2b; TABLE 1). Both materials often have interbedded clay-rich layers that host the sliding surface or failure zone[35,37,74,75]. Slow-moving landslides in weak materials such as soils and damaged sedimentary layers deform by flow-type processes, frictional sliding or lateral-spreading mechanisms[27]. However, some slow-moving landslides are also found in highly weathered metamorphic rocks[59,60,76] (TABLE 1), where the presence of clay layers are not reported. In weathered metamorphic rocks, deformation mechanisms can include toppling and creep and do not always have a

Table 1 | **Metrics of some of the most studied slow-moving landslides in the world**

Site	Velocity (m year^{-1})	Dominant material	Presence of clay	Area and maximum depth	Slope	Dominant forcings
Earthflow						
La Montagna, Italy[80]	0.4–92	Cenozoic flysch	+	0.2 km^2	7°	Groundwater
Northern California, USA[20,25,35,42,45,47,65,84,140,185,186,190,191]	0.4–4.2	Mesozoic metasediments	+	10^4–10^6 m^2	10–25°	Groundwater (seasonal and interannual rainfall)
Oak Ridge, USA[66,192]	2.15	Mesozoic metasediments	+	0.35 km^2	17°	Groundwater (rainfall)
Portuguese Bend, USA[63,118]	1	Cenozoic shales, tuffaceous shales and volcanics	+	1 km^2	6°	Coastal erosion, groundwater, anthropogenic loading
Raukumara, New Zealand[69,93]	6	Cenozoic argillite	+	0.03 km^2	10°	Groundwater (cyclones)
Central San Andreas Fault, USA[64]	0–0.25	Mesozoic metasediments	+	0.003–2 km^2	18°	Groundwater (seasonal rainfall), earthquakes
Slumgullion, USA[22,32–34,68,193]	0.5–8	Weathered Cenozoic lava	+	1.8 km^2, 27 m	8°	Groundwater (snowmelt, rainfall)
Super-Sauze and La Valette, France[26,46,55,85,194]	0.01–0.4 m day^{-1}	Mesozoic marls	+	0.2 km^2, 10 m	25°	Groundwater
Complex flow/slide						
Cleveland Corral, USA[6]	1	Colluvium and former landslide deposits	+	0.05 km^2	19°	Groundwater
Corvara, Italy[56,195]	0.16–24	Mesozoic clayey silt or silty clay material	+	2.5 km^2, 48 m	17°	Groundwater (rainfall, snowmelt)
Harmalière, France[13,57,131]	0.1 m year^{-1} to 50 m month^{-1}	Quaternary glacio-lacustrine deposits	+	1 km^2, 50 m	15°	Groundwater (seasonal rainfall, snowmelt)
Hollin Hill, England[131,177,196]	3.5	Mesozoic mudstone	+	10^5 m^2	12°	Groundwater (rainfall)
Pont-Bourquin, Switzerland[37,54,106,170]	0.05 m day^{-1}	Mesozoic shales	+	0.4 km^2	25°	Groundwater (rainfall, snowmelt)
Tessina, Italy[62,197]	1–8	Cenozoic flysch	+	0.6 km^2, 30 m	12°	Groundwater
Utiku, New Zealand[198]	0.02 m day^{-1} to 0.02 m year^{-1}	Cenozoic sandstones and mudstones	+	2 km^2, 65 m	10°	Groundwater
Slide						
Alani-Paty, USA[199]	0.2	Clayey rich debris	+	0.03 km^2	9°	Groundwater (seasonal rainfall)
Cromwell Gorge, New Zealand[71,200]	0.002–0.005	Mesozoic micaschists	–	1.5 km^2, 160 m	21°	Groundwater (rainfall)
Huangtupo, Three Gorges Reservoir, China[15,92,108,109]	0.02–1	Mesozoic mudstones to argillaceous limestones	+	1.3 km^2, 92 m	8–15°	Groundwater (rainfall, lake infill)
Ikoma, DR Congo[16]	3	Weathered tertiary and Quaternary basaltic layers	+	0.2 km^2	9°	Weathering, groundwater (annual rainfall)
Johnson Creek, USA[67]	0.06	Cenozoic mudstone to sandstone	+	0.1 km^2	11°	Groundwater, earthquakes
Kahrod, Iran[73]	0.3	Jurassic brecciated sandstone and shale	+	1.5 km^2, 70 m	25°	River sapping
La Clapière, France[40,42,58,78,201]	5–50	Paleozoic gneiss	–	1 km^2, 160 m	30°	Deglaciation, groundwater
Maca, Peru[23,50,81,82]	0.2–10	Quaternary fluvio-lacustrine and rock avalanche deposits	+	1 km^2, 80 m	11°	Groundwater (seasonal/interannual rainfall), earthquakes, river sapping
Mud Creek, USA[10,202]	0.5	Mesozoic metasediments	+	0.23 km^2	32°	Groundwater (rainfall), coastal erosion
Siguas, Peru[18,44]	35	Cenozoic sediments: siltstones to conglomerates interbedded with sands and ignimbrites	–	1 km^2, 80 m	14°	Groundwater (irrigation)
Vajont, Italy[8,107]	~1 m year^{-1} before collapse in 1963	Mesozoic limestones	–	2 km^2, 250 m	30°	Lake infill

Table 1 (cont.) | **Metrics of some of the most studied slow-moving landslides in the world**

Site	Velocity (m year^{-1})	Dominant material	Presence of clay	Area and maximum depth	Slope	Dominant forcings
Slide (cont.)						
Vallcebre, Spain[61]	0.5	Late Cenozoic to early Cenozoic sediments	+	0.8 km^2	10°	Groundwater (rainfall)
Zentoku, Japan[72,203]	0.05–0.2	Mesozoic weathered crystalline schist	+	2 km^2	28°	Groundwater, earthquakes
Complex slide/topple						
Åknes, Norway[204–206]	0.01–0.4	Palaeozoic orthogneiss	–	0.6 km^2, 70 m	40°	Groundwater
Moosfluh, Switzerland[59,77,130,207]	0.04 m year^{-1} to 0.8 m day^{-1}	Palaeozoic metamorphic and magmatic rocks	–	1.3 km^2, 175 m	35°	Deglaciation
Séchilienne, France[36,60,79,208,209]	1	Paleozoic fractured micaschists	–	2.1 km^2, 200 m	35°	Groundwater, deglaciation

The velocity is taken as the typical velocity registered in the central body of the landslide. The size of each landslide is given as the surface area and, when available, the maximum depth. The slope is calculated as the mean slope gradient over a longitudinal profile crossing the entire landslide.

clear failure zone at depth[60]. Toppling occurs when rocks have pre-existing near-vertical fractures[77] and a high slope gradient (≥30°; TABLE 1). Steep rockslides are often initiated following a deglaciation, with slow motion that can occur over 10,000-year timescales[76,78,79]. In general, despite differences in the geology of slow-moving landslides, weak and/or altered material is always associated with slow motion.

Slow-moving-landslide velocities are found to be highly variable in space and time. For instance, La Montagna earthflow, Italy, displays velocities varying spatially from 0.4 to 92 m year^{-1} (REF.[80]), while the Maca landslide, Peru, displays velocities that can vary temporally from 0.01 to 10 m year^{-1} in a single location[81,82]. Nearly all slow-moving landslides exhibit daily, seasonal and yearly velocity variations, with large changes in velocity sometimes observed during a single year[33,83,84]. For example, the Super-Sauze earthflow, France, can stop moving in the dry season (between July and September) and then move at rates of 0.4 m day^{-1} during the wet season[85]. Owing to the wide changes in kinematics in space and time, it is difficult to define the mean velocity of a single landslide. As such, we report the maximum annual velocity measured on the central part of the landslide body (TABLE 1). Most of the slow-moving landslides described in this Review move at maximum rates between 0.3 and 10 m year^{-1} (FIG. 2c), which corresponds with deformation that is easily recognizable by analysing the surface morphology or damages on human infrastructure. In addition, the velocities of most slow-moving landslides described here are within the precision of common geodetic methods (such as the Global Navigation Satellite System; GNSS) and, therefore, provide the opportunity to investigate landslide mechanics and forcing factors.

Forcings and mechanisms

A variety of internal and external factors are known to drive landslide dynamics (FIG. 3), resulting in changes in the mechanical properties of the material and/or landslide acceleration or collapse (FIG. 4). Internal and external forcings include upslope loading of the landslide from deposition of new material[7,44,63,86] (FIG. 4a); changes in groundwater from rainfall or snowmelt[10,25,32–34,36,47,87–91] (FIG. 4b); changes in the water level within lakes, reservoirs and rivers, particularly during impoundments[8,15,86,92] (FIG. 4c); shaking from earthquakes[3,23,50] (FIG. 4d); deforestation[93]; and debuttressing of the landslide toe from river erosion[66,73], man-made infrastructure[86] or glacier retreat[78,79] (FIG. 4e). By reviewing how landslide properties relate to the different forcings, we provide a better understanding of the mechanical controls on landslide processes.

For simplicity, let us consider a landslide with a sliding surface at depth. The parameters that influence slope stability are derived from equations originating from critical-state soil mechanics with a Mohr–Coulomb failure criterion[94]. The Mohr–Coulomb failure criterion states that failure, or motion, will occur when the combination of shear and normal stresses acting on any point of a material reaches a threshold value that is controlled by some material properties (for example, cohesion and angle of internal friction).

Stability is generally described with a factor of safety (FoS), which is calculated as the ratio between the resisting forces (shear strength) and the driving forces (shear stress) acting on a shear plane at the bottom interface between the landslide mass and the stable material. Stability is expected when FoS >1, whereas instability occurs when FoS <1. When FoS = 1, stability is at the limit equilibrium. Landslide forcings act to decrease the FoS and either trigger the initial failure or induce the acceleration of already failed slopes. Below, we further describe how changes in the driving or resisting stresses can influence the behaviour of slow-moving landslides.

Decreasing the strength. Changes in the shear strength of landslide material is a primary cause of failure and/or acceleration. Decreased shear strength can occur from weathering and alteration (either mechanical or chemical)[16,95,96], reduction of the effective normal stress, diminution of the soil cohesion (the cohesion of a granular material results from capillary force, electrostatic bonds and grain cementation) and fluidization of subsurface layers. All these processes, in combination with gravitational stresses, can lead to progressive damage of

the landslide material, development of fractures and, ultimately, coalescence into a shear band[8] (1 in FIG. 3). The shear zones might then become susceptible to low-magnitude external forcings (such as small rain events following periods of relative quiescence[13,97]) that result in landslide triggering and acceleration.

In addition to changes in strength induced by weathering and material damage, hydrological processes,

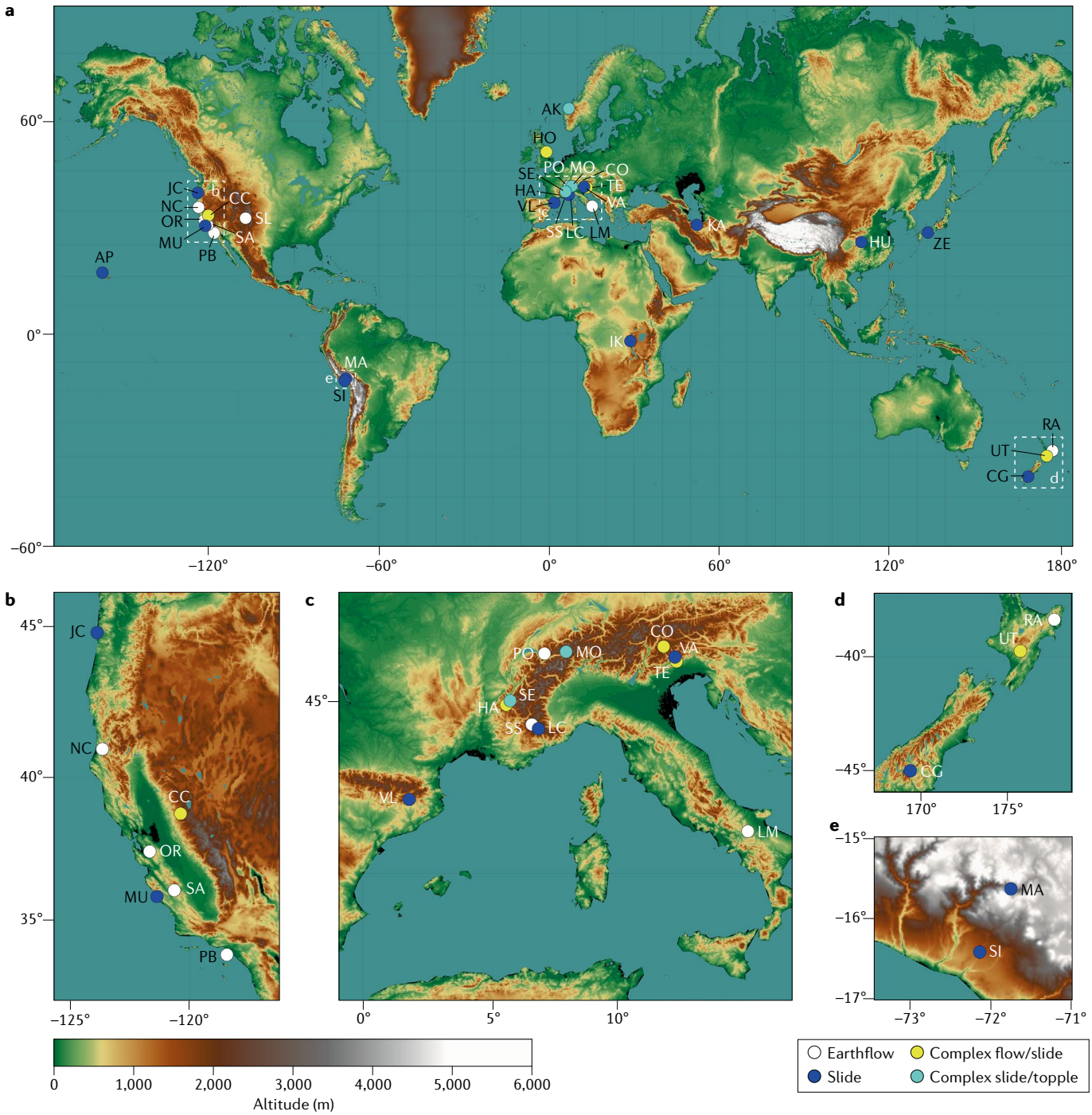

Fig. 1 | **The location of some of the best studied slow-moving landslides.** A selection of slow-moving landslides reported worldwide, including AK, Åknes, Norway; AP, Alani-Paty, USA; HO, Hollin Hill, UK; HU, Huangtupo, Three Gorges Reservoir, China; IK, Ikoma, DR Congo; KA, Kahrod, Iran; SL, Slumgullion, USA; and ZE, Zentoku, Japan (panel **a**). Multiple landslides have been observed in the western USA (panel **b**): CC, Cleveland Corral; JC, Johnson Creek; MU, Mud Creek; NC, northern California; OR, Oak Ridge; PB, Portuguese Bend; and SA, Central San Andreas Fault; Europe (panel **c**): CO, Corvara, Italy; HA, Harmalière, France; LC, La Clapière, France; LM, La Montagna, Italy; MO, Moosfluh, Switzerland; PO, Pont-Bourquin, Switzerland; SE, Séchilienne, France; SS, Super-Sauze, La Valette, France; TE, Tessina, Italy; VA, Vajont, Italy; and VL, Vallcebre, Spain; New Zealand (panel **d**): CG, Cromwell Gorge; RA, Raukumara; and UT, Utiku; and Peru (panel **e**): MA, Maca and SI, Siguas. The distribution of slow-moving landslides highlights that they are typically only reported in developed countries. Different types of slow-moving landslides (earthflow, slide, complex flow/slide and complex slide/topple) are displayed in the legend.

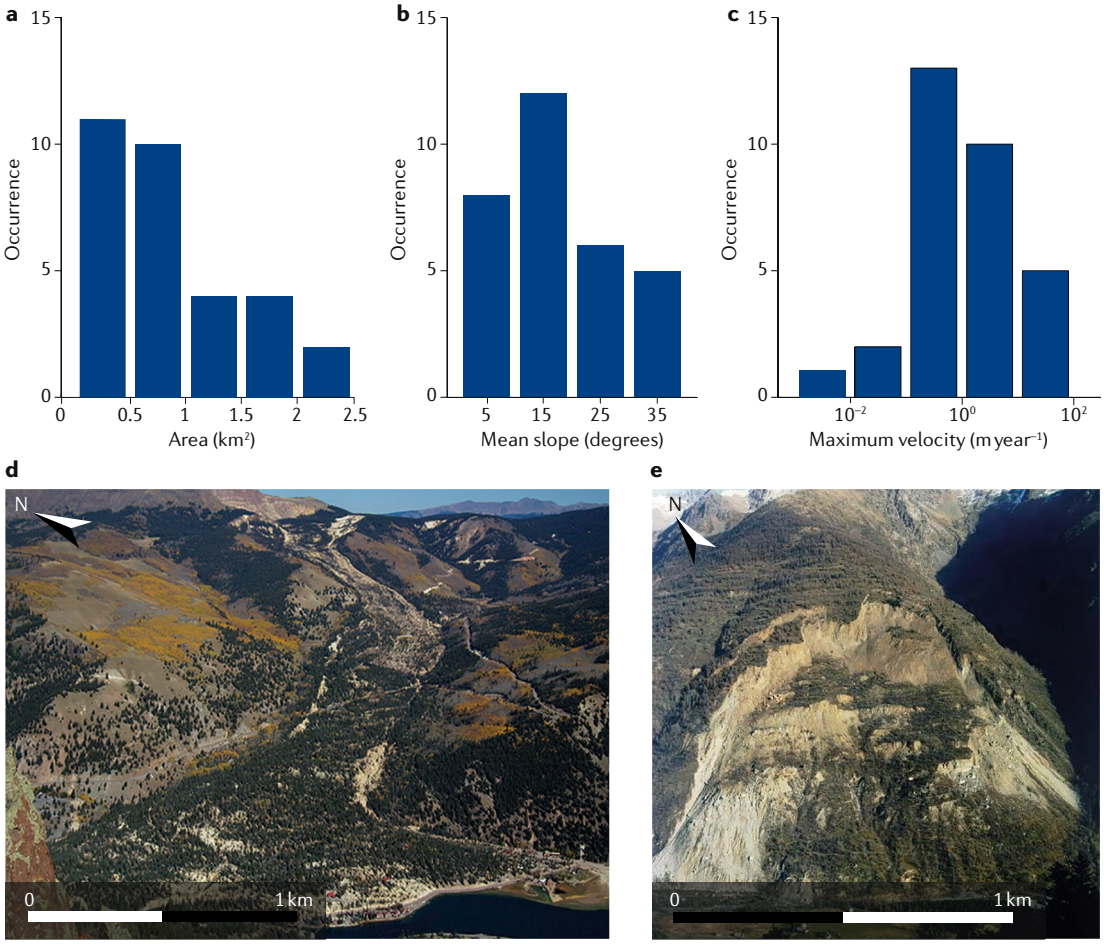

Fig. 2 | **Key characteristics of the compiled landslide database.** Histograms reveal the distribution of landslide area (panel **a**), mean slope (panel **b**) and maximum landslide velocities (panel **c**) in the compiled database. Photos of the Slumgullion debris slide, USA (panel **d**), and the La Clapière rock slide, France (panel **e**), provide examples of slow-moving landslides. Photograph panel **d** by William Schulz, US Geological Survey. Image panel **e** courtesy of GeoAzur.

such as water infiltration and compression or extension of saturated landslide materials, result in shear-strength variations. Hydrologically induced strength changes primarily occur because of variations in pore-water pressure and, correspondingly, effective normal stress. As such, strength changes depend on the water-saturation level of the hillslope material. For example, when the material is not fully saturated, suction forces from capillary effects and clay swelling in the lateral shear surfaces can increase shear strength and help stabilize a hillslope[35,98]. However, when the material is nearly or fully saturated, an increase in pore-water pressure induces a loss of cohesion, along with a decrease of the effective normal stress and, consequently, causes a reduction in the shear strength of the landslide material (possibly leading to liquefaction)[99]. The magnitude of the resulting variations in shear strength depends on the drainage conditions of the slope. If the slope has 'drained' conditions, water can flow out of the landslide mass before excess pore-water pressures develop. The opposite is true for 'undrained' conditions, where a rapid increase of stress owing to a specific loading such as water infiltration, with respect to the time required for the water to be drained, in loose, nearly saturated fine-grained formations leads to the build-up of excess pore-water pressure and, subsequently, to a dramatic decrease of the effective normal stress[100].

The infiltration of water into a hillslope can have several origins. Rainfall and snowmelt (2.1 in FIG. 3) and anthropogenic irrigation[18] (2.2 in FIG. 3) can infiltrate through the hillslope matrix[25,49,87,91,101–103] (FIGS 3,4b) or through preferential flow paths, such as fissures and cracks generated by the landslide activity[38,104–106] (1 and 2.3 in FIG. 3). Variations in atmospheric pressure, for example, atmospheric tides, can also cause vertical migration of the groundwater within the landslide. At the Slumgullion landslide, USA, daily variations in atmospheric pressure of less than 1 kPa lead to variations in landslide velocity from less than 1 mm day^{-1} (higher atmospheric pressure) to more than 2–3 mm day^{-1} (lower atmospheric pressure)[33]. Changes in the water level of a lake or reservoir (natural or man-made) at the hillslope toe can also generate variations in the groundwater levels within the landslide body and, therefore, impact landslide kinematics[8,15,71,92,107–109] (FIG. 4c and 2.4 in FIG. 3).

The relationships between rainfall and/or snowmelt and landslide acceleration has been documented in many regions worldwide[34,56,61,87,89,110–112] and indicate that the highest velocities are generally observed during

periods of intense or long-lasting rainfall (such as wet seasons, monsoons and/or summer storms) and during periods of high snowmelt discharge (winter to spring). For example, the Slumgullion landslide, USA, attains its maximum velocities of ~10 m year^{-1} (170% the average annual rate) during peak snowmelt[34]. Furthermore, the Maca landslide, Peru, accommodates 90% of its 1–10 m annual displacement within the five months of the rainy season[81]. In the same way, but with a much lower magnitude, the Charlaix landslide, French western Alps, has slide velocities of 13–16 cm year^{-1} from November to March and 0–2.5 cm year^{-1} from April to October[113]. The direct relationship between rainfall and/or snowmelt-induced water infiltration and landslide occurrence and acceleration led to the proposal of early-warning systems for shallow (generally no more than a few metres), catastrophic landslides based on regional-specific rainfall intensity and duration thresholds[88,114,115]. However, rainfall-based early-warning systems are not appropriate for deep-seated (thickness >3 m), slow-moving landslides, owing to the increased complexity of their subsurface hydrological network relative to shallow catastrophic landslides (for which the early-warning systems were designed)[26,116].

Water infiltration can also originate from man-made operations, such as irrigation for large-scale agriculture or personal use and from sewage and drainage systems[18,63,117] (2.2 in FIG. 3). For instance, massive irrigation for farming in the desert of Tacama, South Peru, led to the reactivation of huge slow-moving landslides in the two distinct valleys of Siguas and Vitor[18]. In the arid environment of the Tacama desert, a 20-year delay between the onset of irrigation and the initiation of landsliding was observed, which was interpreted as the time needed to develop high pore-water pressures[18]. Ultimately, migration of the Punillo Sur landslide generated displacements of ~300 m in 30 years. In addition, the Portuguese Bend landslide, USA (TABLE 1), was reactivated in the mid-1950s following gravitational loading at the head of the landslide by a highway fill up to 20 m thick and water infiltration originating from rainfall, waste water and surface watering[63]. Since then, the landslide has remained active, owing to rainfall and additional waste water from nearby residences[63,118].

Further insights into the influence of man-made operations on the motion of landslides can be gained by studying the pore-water geochemistry of different landslides, such as the clayey Manaihan landslide in eastern Belgium. The Manaihan landslide, which had been dormant for around 1,600 years, was reactivated twice, first in the 1970s and then again in 1998 (with motion continuing to the present day). The second reactivation was triggered by a broken sewage pipe and heavy rainfall[117]. Interestingly, geochemical analysis on different industrial sewage waters showed enrichment in monovalent ions (such as Na^+ and K^+), which might have promoted the landslide movement[117,119]. Experimental studies conducted on quick clays in Norway[119,120] showed that replacing in situ cations by cations of smaller hydrated radii (bigger cations with an associated lower water-ion volume) decreased the thickness of the electrical diffuse double layer between clay particles and improved the undrained and remoulded shear strength, and the Atterberg liquid limit, of the tested soils, thus inhibiting the rapid motion or catastrophic failure of landslides. The influence of pore-water geochemistry and clay mineralogy have been long investigated for clay liner applications but remain poorly reported in landslide investigation, with the exception of quick clay[117,119,121,122]. As such, it remains an area of prospective research.

Deforestation (3 in FIG. 3) can also cause drops in the shear strength of landslide material and promote landsliding in several ways. First, vegetation favours transpiration and, as such, reduces the amount of water

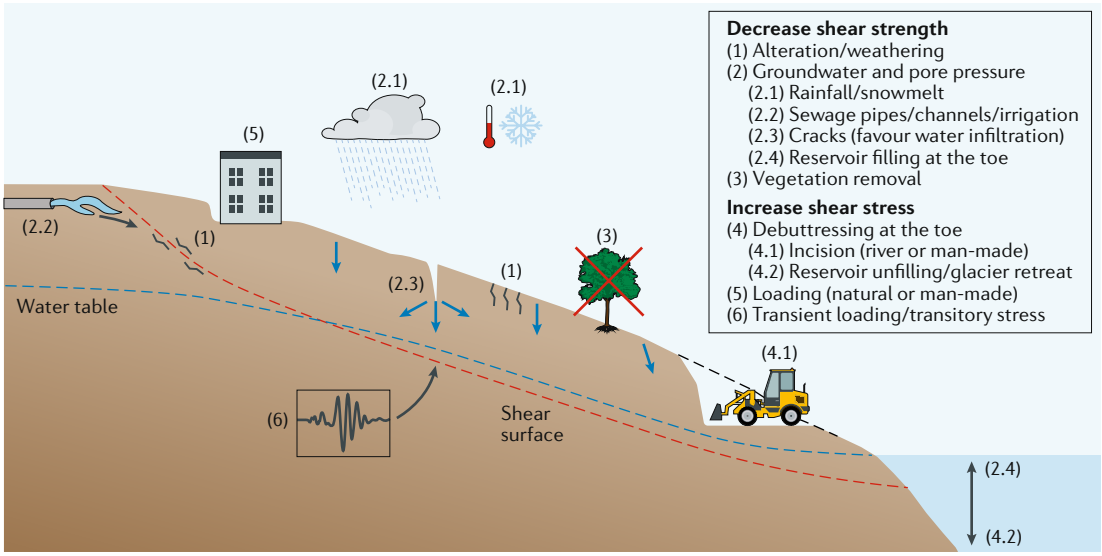

Fig. 3 | **Schematic demonstrating the possible forcings of landslides.** Forcings that may lead to a decrease in the shear strength of the landslide material, including alteration and/or weathering, removal of vegetation and hydrological processes from rainfall infiltration, lake infill or material property changes during earthquakes. Alternative forcings might lead to increased shear stress acting on the landslide material, including debuttressing at the toe, anthropogenic loading or natural material deposition, and short-term loading (for example, earthquakes). Sketch adapted from REF.[86], CC BY 4.0.

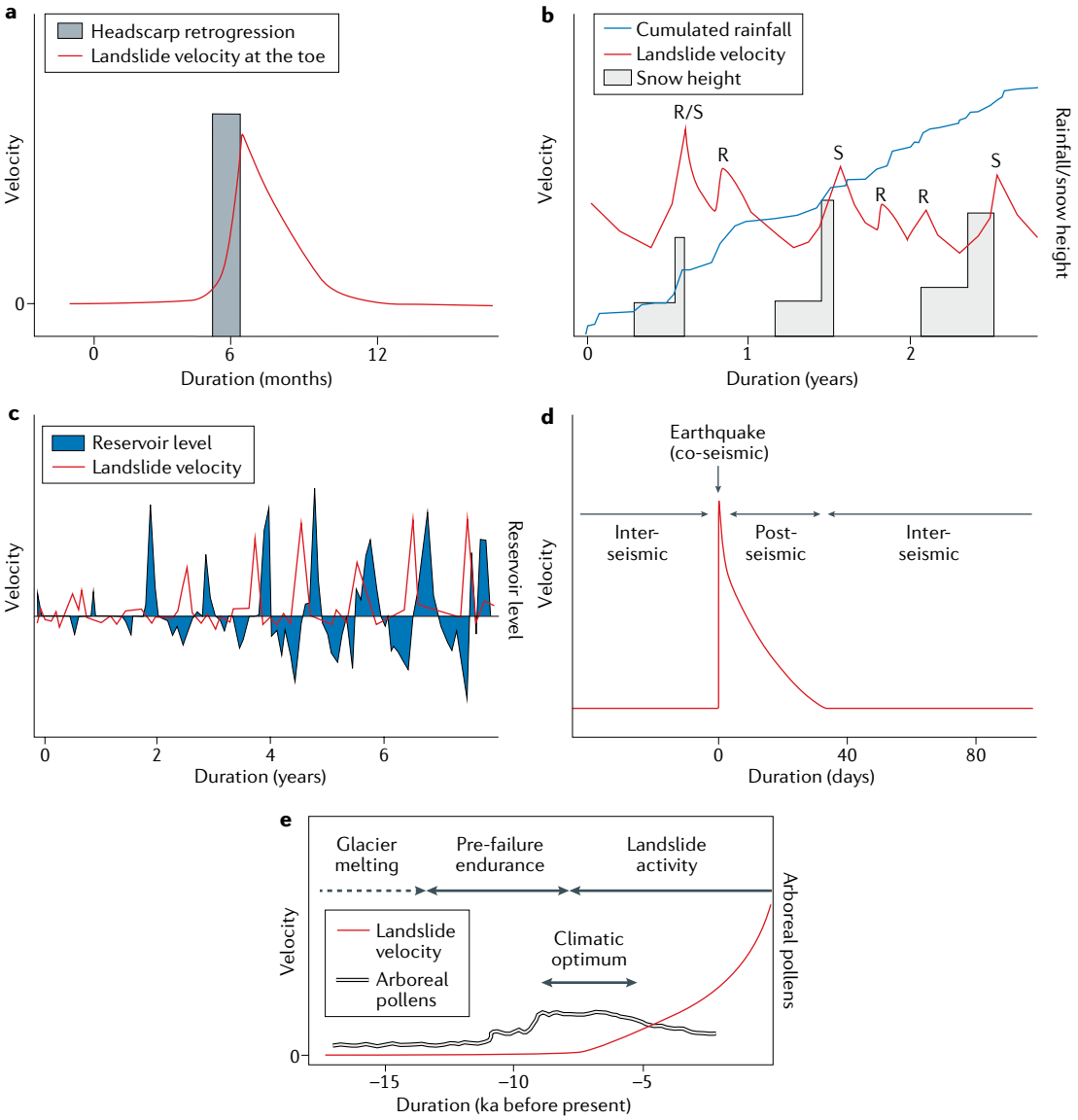

Fig. 4 | **Possible forcings for driving landslide acceleration.** Variations in landslide velocity can be driven by multiple forcings, including loading on the landslide body (for example, material supply from landslide headscarp retrogression) (panel **a**); variations in pore pressure driven by rainfall and/or snowmelt (R refers to rainfall forcing, S to snowmelt forcing and R/S to mixed forcings) (panel **b**); reservoir filling, which can also lead to variations in pore pressure (panel **c**); earthquakes, causing transient loading and variations of the material damage (panel **d**); and debuttressing at the toe from deglaciation (panel **e**). ka, kilo annum, that is, thousand years. Panel **a** adapted from REF.[18], Springer Nature Limited. Panel **b** adapted with permission from REF.[68], Elsevier. Panel **c** adapted with permission from REF.[92], Elsevier. Panel **e** adapted with permission from REF.[79], Elsevier.

infiltrating the subsurface, which has the largest impact for deep-seated landslides. Second, roots absorb water from the subsurface and increase suction, which stabilizes shallow landslides. Third, the spatial distribution of the root network into the ground mechanically increases shear strength[99] and, therefore, reduces the probability of shallow landslides initiating.

A decrease in strength can also result from slip-dependent or rate-dependent changes in material properties and from stress changes during earthquakes. Some landslides exhibit rate-weakening friction, where the frictional strength decreases as the landslide velocity increases[123,124]. The origin of rate-weakening behaviour is still debated and might reflect the pure frictional behaviour of the sliding surface or the plastic deformation of junctions in the bulk material[125]. Critically, rate-weakening friction promotes acceleration that sometimes ends in catastrophic failure[51,124]. Stress changes during earthquakes can also reduce the shear strength. Indeed, many studies have explored the role of fluids during seismic shaking and have found that fluid migration, following an earthquake, occurs because of changes in permeability[126] and could result in a rise in the pore-water pressure, owing to undrained soil conditions[127]. In addition, grain crushing in the shear band following seismic shaking can lead to liquefaction of the sliding surface[128,129].

Quantification of the different earthquake-related forcing mechanisms remains challenging, demonstrating that more observations of slow-moving landslides accelerated by earthquakes are required to study the mechanical implications of seismic shaking.

Increasing the shear stress. Changes in the FoS and, therefore, the probability of landslide motion might also occur through changes in the shear stress of a hillslope. Increased shear stress can result from oversteepening of the slope, debuttressing of the toe (4.1 and 4.2 in FIG. 3) or upslope loading (5 in FIG. 3). For example, several deep-seated landslides, which occur along the flanks of steep mountain valleys (such as the La Clapière and Séchilienne landslides in France[78,79]), were initiated following the most recent deglaciation period (~10,000 years ago) and, thus, removal of material from the toe of the landslide. Similar debuttressing effects at the toe of landslides owing to deglaciation or river incision have also been observed on the Kahrod landslide in Iran[73], on the Oak Ridge earthflow in the USA[66] and on the Moosfluh landslide in Switzerland[77,130].

Internal or external structural changes following natural or man-made mass redistribution can also lead to increased shear stress and generally occur in several (at least two) stages (FIG. 3). First, a phase of erosion or man-made surface changes in the upper part of the landslide transports material down to an accumulation zone. The resulting growth of soil thickness at the accumulation zone can induce an increase in the driving shear stress acting on the landslide body, which can cause undrained loading and trigger acceleration and/or a transition from sliding to flowing[48]. Landslide acceleration following loading has been observed at several sites. For example, the Silt Creek landslide, USA, was reactivated due to undrained loading following two debris flows that deposited 10 m of material onto the upper part of the landslide's transport zone[7]. Similar observations have been made at other landslides around the world[13,18,44,63], including the Harmalière landslide, France, the Portuguese Bend landslide, USA or the Siguas and Punillo landslides, Peru, where new material supplied by the regression of the headscarp led to acceleration of the main landslide body (displacements increased by ~50 m in 3–5 weeks)[13,18].

A transition from sliding to flowing owing to structural changes in the landslide body has been observed at many landslides (such as the Harmalière, Hollin Hill, Pont-Bourquin and Super-Sauze landslides; FIG. 1). The transition to flowing can occur because the increase in shear stress resulting from material deposition acts to decrease the water content required to trigger a transition from sliding to flowing[131]. However, the increased driving stress owing to loading is not always sufficient to trigger landslide acceleration. In some cases (often in drained conditions), the increase in normal stress from the additional material weight acts to cancel out the increased driving stress and results in negligible net change in landslide shear strength.

Short-term transient loading such as ground shaking from earthquakes can also dynamically increase the stress on a landslide shear band and, therefore, lead to a transient decrease of the FoS[132] (6 in FIG. 3). Dynamic loading can explain the co-seismic acceleration of slow-moving landslides such as the Maca landslide in Peru, which displayed ~2 cm of co-seismic slip during a nearby Mw 6.0 earthquake[43,50] (FIG. 4d). The co-seismic motion was followed by ~6 cm post-seismic motion over 5 weeks, where no notable rainfall events occurred. The post-seismic motion of the Maca landslide was explained mechanically using rate-and-state friction laws[50,51]. However the viscoplastic properties of clay layers and the effects of fluids under seismic forcing must be taken into account to better understand the mechanics of slow-moving landslides during earthquakes.

Recent studies have also shown that complex combinations of the different forcings, such as rainfall combined with earthquakes or debuttressing, control the occurrence of rapid landslides[133] and rockfalls[134], as well as the kinematics of slow-moving landslides[23,79]. For slow-moving landslides, earthquakes and rainfall together produce larger motions than the two forcings individually, as earthquakes can further damage the landslide material and increase water-infiltration capacity, which, in turn, leads to an additional decrease in the effective normal stress[23]. Similarly, the joint action of debuttressing and increased rainfall promotes landslide motion[79]. The interplay of different forcings illustrates the complexity of landslide mechanics. Furthermore, in many situations, the same forcing can lead to variations in both the shear strength and the normal stress acting on a landslide slip surface. We, therefore, emphasize the necessity to instrument slow-moving landslides with diverse equipment (for example, piezometers, seismometers, and ground-surface and depth-displacement sensors) to extract various landslide properties (such as velocity, damage and pore-water pressure) and for studying landslide mechanics in general. Owing to the inherently heterogeneous properties of landslides (such as their velocity, water flow, type of material and geometry), instrumentation needs to be spatially and temporally extensive.

From slow to rapid landslides

In this Review, we have focused on slow-moving landslides that have remained active for many years, sometimes as long as 1,000 years[135–137]. However, it is also possible for slow-moving landslides to accelerate rapidly, move unusually large distances and even fail catastrophically[8–14,66] (schematic shown in FIG. 5a). The transition from slow to rapid movements can occur in any lithology; for example, lacustrine deposits[13], metasediments[10] or metamorphic rocks[8,9,14]. However, the duration of landslide acceleration is typically longer in stiff rocks. For instance, landslide acceleration can occur over several months in metamorphic rocks[8,9,14], but might last only days in clay-rich sediments[13]. Landslide acceleration over timescales spanning days to months presents both opportunities and challenges for pre-failure detection.

The mechanisms driving the transition from slow to rapid behaviour have been widely investigated and include a switch from shear-induced dilatant strengthening to contraction weakening[76,100,138–141] (FIG. 5b), a stress-induced decrease in material viscosity[37,131,142]

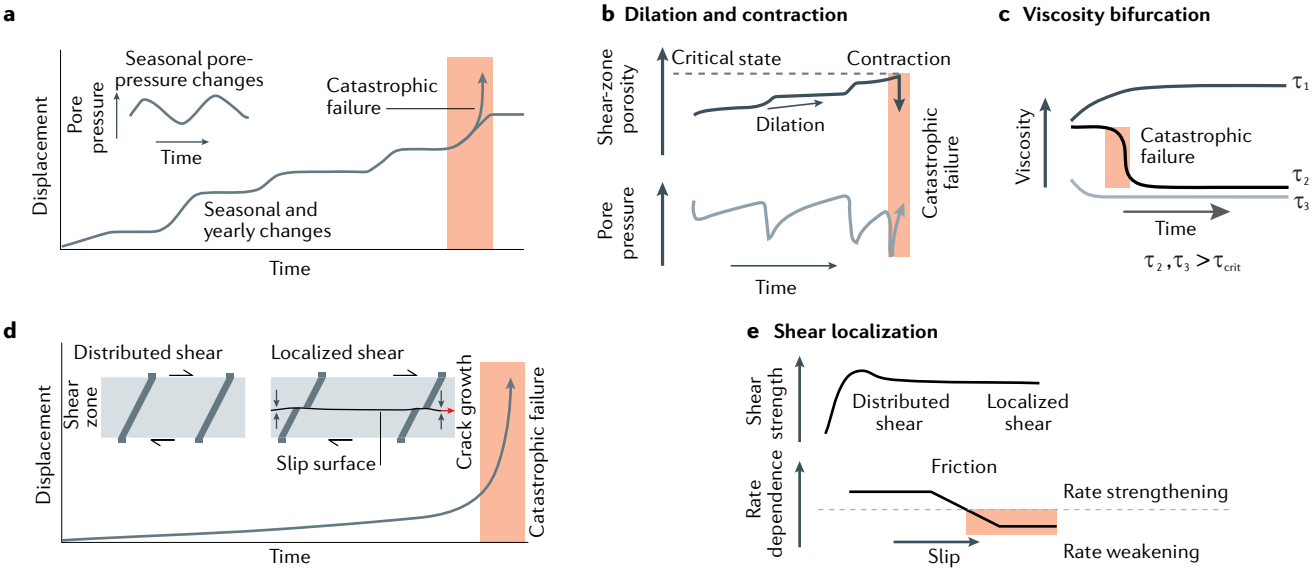

Fig. 5 | **Schematics of landslide displacement and their associated mechanisms during the transition from slow to fast motion. a** | Time series of complex yearly and seasonal displacement and a transition to catastrophic failure. Inset shows an example of the precipitation-induced pore-water-pressure changes that drive the seasonal landslide motion. **b** | Dilatant strengthening and contraction weakening, represented by the shear-zone porosity and pore-water-pressure changes that result in slip events. Catastrophic failure occurs at the critical state line. **c** | Viscosity bifurcation time series, which displays a rapid reduction in viscosity when the stress exceeds a critical value (τ_{crit}). **d** | Typical creep-to-failure time series, where the landslide accelerates at a constant rate. Shear zones with distributed shear, which occurs during the onset of motion, and localized shear, which occurs during the runaway final acceleration, are displayed in the insets. **e** | Shear strength and rate-dependent friction changes during shear localization, where the grey dashed line represents the transition from rate-strengthening to rate-weakening behaviour. In all figures, the orange box highlights the transition from slow motion to catastrophic failure. Panel **b** adapted with permission from REF.[138], Geological society of America. Panel **c** adapted with permission from REF.[142], APS. Panels **d** and **e** adapted with permission from REF.[210], Annual Reviews.

(FIG. 5c) or strain localization[143–145] (FIG. 5d,e). Shear-induced dilation or contraction cause changes in pore-water pressure during sliding that can control the failure mode (FIG. 5b). Dilatant strengthening (increasing porosity) during slip events causes a decrease in pore-water pressure and an increase in shear strength, which help prevent runaway acceleration, while contraction weakening (decreasing porosity) causes pore-water pressure to rise and promotes runaway acceleration[100,138,140,141,146]. Whether the landslide material dilates or contracts upon sliding depends on its initial compaction state. Densely packed materials tend to dilate during sliding, while loose materials tend to contract. A transition from dilation to contraction (slow to rapid motion) can occur when the material reaches its critical-state porosity (typically, the maximum porosity). During this transition, if the rise in pore-water pressure equals or exceeds the overburden stress, liquefaction will occur, leading to large, fast displacements and long runout distances[141,147]. For example, the basal surface of the catastrophic Oso landslide, USA, which killed 43 people and destroyed 35 homes, liquefied during failure, resulting in rapid motion and high mobility[141,147].

In addition, liquefaction can also occur from small stress changes[37], owing to a bifurcation in viscosity or shear modulus of clay layers within landslides[131,142] (FIG. 5c). Stress-induced liquefaction has resulted in the rapid acceleration and, correspondingly, large displacements of several slow-moving landslides worldwide, such as the Harmalière and Super-Sauze landslides in France[131]. Finally, strain localization, which is the consequence of progressive damage resulting from subcritical crack growth and leads to the formation of a narrow shear band along which sliding can occur (FIG. 5d,e), can trigger constant acceleration of the landslide mass (FIG. 5d).

Owing to the diversity in landslide behaviours, attempts have been made to unify the mechanical laws that govern both slow and rapid motions[140]. While the critical-state soil-mechanics framework dominates the landslide literature, fault-mechanics-based rate-and-state friction theory provides another framework that can be used to describe slow and fast landslide motion[50,51,107,124,148]. The empirical rate-and-state friction law predicts that slow landslide motion will occur if the landslide sliding surface becomes stronger with increased slip or velocity. Alternatively, if the sliding surface becomes weaker with increased slip or velocity and the landslide dimensions exceed a critical size, then there is potential for runaway acceleration[149,150]. The slip-dependent or rate-dependent frictional properties can result from inherent material properties[123,151], strain localization[144,145] and can be further enhanced by shear-induced changes in pore-water pressure[140,152–154]. However, more work is required to better connect fault-mechanics frameworks to slow-moving and fast-moving landslides. We emphasize the need for laboratory-based studies to measure the rate-dependent

and state-dependent frictional properties of landslide materials at appropriate stress conditions[76,124], alongside field-based investigations using high-resolution kinematic measurements to constrain rate-and-state friction models. In particular, new data and measurements are required for cases where slip pulses are triggered by stress changes resulting from earthquakes or rainfall[7,50,51].

It is necessary to develop ways to determine, in advance, whether a landslide will accelerate rapidly or continue to slide slowly. One common approach is to examine the time series of a precursory signal, such as displacement or strain, that precedes runaway acceleration[12,143,155,156]. Accelerating rates of the precursory signal can be approximated by an empirical relation that describes the acceleration as a function of the rate, commonly referred to as the Failure Forecast Method (FFM) or Voight's law, which describes the final stages of the tertiary creep of brittle materials (FIG. 5d). For landslides, the FFM is often performed by analysing the form of the inverse velocity time series. In many cases, it has been shown, often retrospectively, that the timing of catastrophic landslide failure can be forecast by fitting a linear function to the inverse velocity ($1/v$) time series and identifying the point at which $1/v$ approaches zero.

The FFM has been applied to back analyse the 1963 Vajont landslide[107,157], showing that catastrophic failure could have been forecast almost a month in advance. The potential of failure prediction from pre-failure monitoring has led some countries, and private companies (like those that operate mines and quarries), to install in situ monitoring systems, mostly based on extensometers or geodetical measurements of the surface velocity in vulnerable areas where slow motions have been detected[158–160]. Failure predictions have been applied with varying degrees of success. Back analysis of monitoring data, and the predictions made, demonstrate the importance of the continuous and precise landslide-displacement monitoring[158–160].

It must be noted that precursory signals before landslide collapse are not limited to surface displacement or strain. For instance, the increase in endogenous microearthquakes[156,161,162] and a drop of the material rigidity[23,37,97] have both been shown to be a precursor to landslide acceleration. For example, the Nuugaatsiaq landslide, Greenland, exhibited an inverse power law increase in the rate of endogenous microearthquakes towards failure, consistent with the FFM, although the microearthquakes were triggered only hours before the landslide failure occurred[162]. Similarly, the Pont-Bourquin landslide, Switzerland, exhibited a rapid and important decay of the material rigidity in the 3–5 days before its failure[37]. Both precursory signals can result from material damage or the landslide motion itself.

Further landslide material damage can result from external forcings such as groundwater circulation or nearby shaking from earthquakes[23], with complex interactions between the different forcings. On the Maoxian landslide, China, acceleration during the weeks before the catastrophic failure was triggered by several weeks of above-average rainfall that resulted in high pore-water pressures[163]. However, years of preceding slip and rock damage from nearby earthquakes likely contributed to its ultimate collapse[9]. The range of precursory behaviours outlined here highlights the importance of monitoring some selected slow-moving landslides over long time periods with a wide variety of sensors to understand the processes leading to the rupture.

Summary and future perspectives

Slow-moving landslides around the world are controlled by complex interactions between internal factors, such as the state of the landslide material or pore fluids, and external forcing factors, such as seismicity, river incision or human impact. As a result, landslides display a wide variety of kinematic behaviours that have meaningful implications for both hazards and landscape evolution. The kinematics of slow-moving landslides reveal a range of complex underlying physical parameters, involving the mechanical properties of the material (for example, cohesion, friction and bulk damage), sliding history, pore-water pressure and dynamic loading. The continued development of mechanical models of landslide dynamics is critical to provide a better understanding of the complex interactions that control landslides and, potentially, allow for the prediction of rapid landslides. It is, therefore, important to maintain continuous monitoring networks on well-known landslides over long timescales (several decades) to develop and improve future models of landslide dynamics.

Similarly complex mechanical and kinematic behaviours occur in other geophysical phenomena, such as faults[164], volcanoes[165] and glaciers[166,167]. Much of the deformation associated with these other phenomena is related to rock damage and frictional sliding driven by stress or strain. Thus, investigation of slow-moving landslides, which are relatively easy to monitor compared with volcanic eruptions or earthquakes (owing to their smaller size, shallow depth and persistent motion), offer a natural laboratory that can be used to gain a better understanding of the mechanics of frictional sliding and failure in natural materials[50,51,168]. Recent efforts to apply the fault-mechanics-based rate-and-state friction model to landslides[50,51,76,107], volcanoes[169] and glaciers[166,167] emphasize the similarities between the different systems, and we encourage more collaboration between research based on landslides, volcanoes, glaciers and faults.

Challenges of future landslide research will certainly be directed towards improving monitoring tools, with the aim to get precise, high-frequency and extensive data. However, one of the primary concerns is the cost of instrumentation. Projects using low-cost instruments such as radio-frequency identification[170], fixed optical cameras[38] or low-cost GNSS and unmanned aircraft systems or drones[171] will help mitigate some of the costs. In addition, monitoring of subsurface properties will benefit from the development of dense geophysical sensor layers, either seismometers (associated with recent advances in continuous, passive, seismic-noise-monitoring techniques[23,172]) or resistivimeters[173], which will contribute to advancing understanding and modelling of material damage and groundwater circulation within the landslide body. To this end, recent progress has been made in time-lapse monitoring of 2D and 3D electrical and seismic parameters[174–178].

There is also a need to better understand the chemical effects of groundwater circulation, especially on crack growth and bulk damage, as well as the conditions leading to the fluidization of clay-rich layers[131,141].

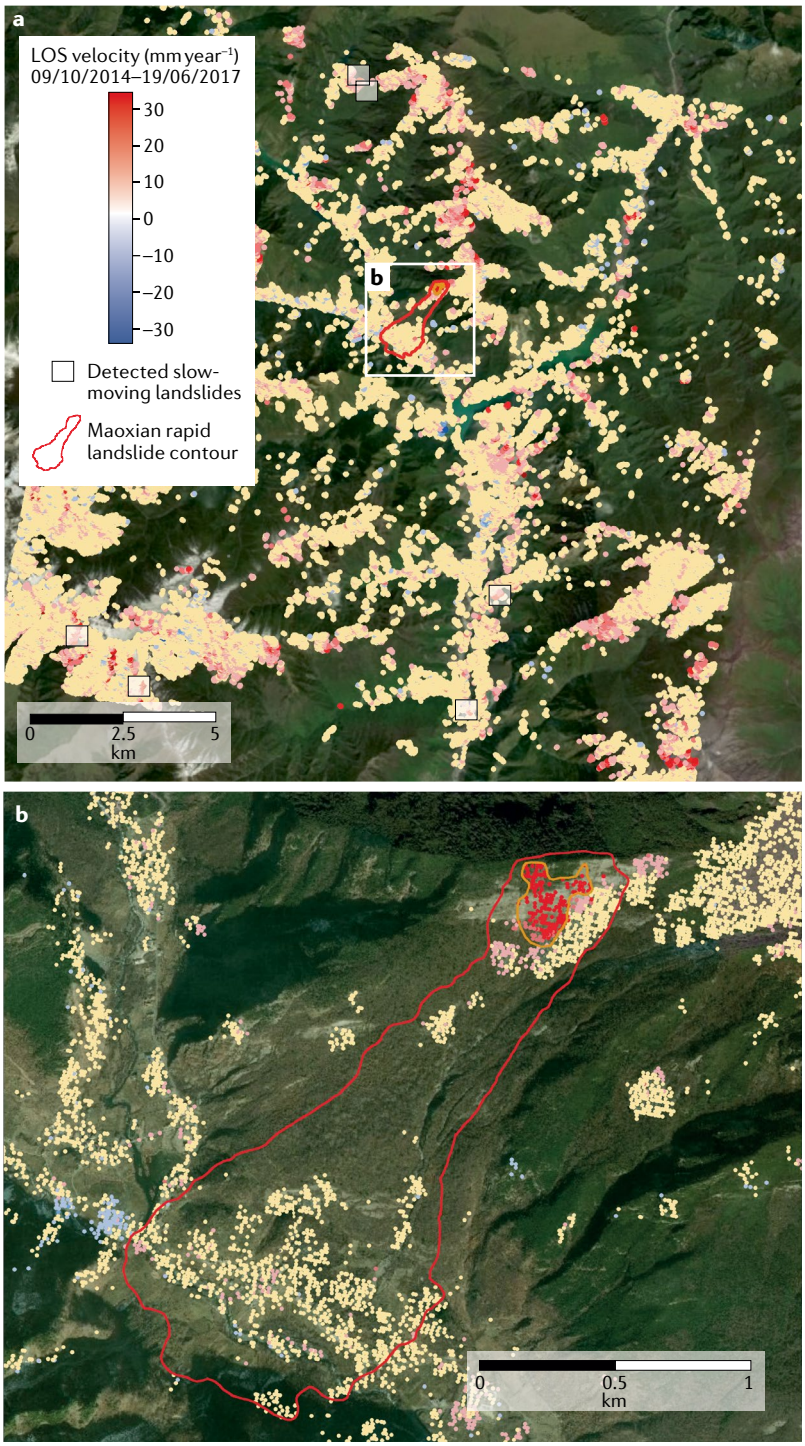

Fig. 6 | **Velocity map of ground motion over 3 years before the collapse of the Maoxian landslide, China. a**,**b** | For each point, a time series of ground motion with time intervals of 12 days is available. Data were acquired by the Copernicus Sentinel-1 radar satellites and the processing provides a velocity in the satellite line-of-sight (LOS) direction (in mm year^{-1}). All data displayed were collected from freely available satellite data. The data present information about the ground velocity before catastrophic landslide failure but also reveal the complexity associated with the large numbers of data gaps and noisy measurements from satellite data that can lead to false alarms. Adapted from REF.[9], CC BY 4.0.

Relatively long time series (decades) of multi-sensor monitoring on slow-moving landslides will be key to obtain a variety of groundwater measurements that can be used to better understand the non-linear response of slow-moving landslides to external forcings and the progressive damage of slow-moving-landslide material with time, especially in response to ongoing climate change[47,179]. Some examples of multi-year monitoring efforts are already underway, such as at the French National Landslide Observatory (OMIV), which has maintained geodetic, seismic and groundwater measurements on several landslides since 2007 (REF.[52]).

Research on slow-moving landslides also helps us characterize behaviours that precede rapid landslides. As such, detection of slow-moving landslides is critical for alert purposes. Major developments are expected in landslide detection, owing to the increasing availability of high spatial and temporal resolution remote-sensing data across the globe[9,12–14,180–183]. Back analysis of various case studies show that landslide acceleration could have been detected from satellite data a few days to weeks before their catastrophic collapse. The use of freely available, high-frequency interferometric synthetic-aperture radar (InSAR) acquisitions, for example, from the Sentinel-1 satellites (minimum acquisition frequency of 6 days), allows for the detection of cm month^{-1} changes in velocity[9,12], whereas the cross-correlation of freely available optical images from high-frequency satellite acquisitions such as Sentinel-2, Landsat 7/8 and Planet (acquisition frequencies of 5, 8 and 1 days, respectively) allows for the detection of abrupt changes in velocity of ~1 m day^{-1} (REF.[13]).

However, landslide forecasting from satellite data suffers from several limitations. First, forecasting will not work with satellite-based remote-sensing methods if the transition from slow to fast motion happens over days or less, or if the signals are further obscured by seasonal effects[13,162,184]. Second, the signal can be masked by the noise of the satellite measurements. Third, data gaps always exist, owing to clouds, snow cover, topography, and vegetation (FIG. 6). Fourth, the complex nature of landslide pre-failure motion does not always exhibit a unique time-dependent behaviour, which provides additional challenges for landslide prediction. For instance, the InSAR time series of the 2017 Mud Creek landslide, USA, did not indicate a clear transition to runaway acceleration as defined by the FFM, although the landslide did exhibit rapid acceleration and relatively high velocities (maximum rates up to 1.5 m year^{-1}) compared with previous years (maximum rates between 0.1 and 0.5 m year^{-1})[10]. The Mud Creek landslide highlights the necessity to establish long-term monitoring of landslide kinematics, which can be used to search for and identify 'unusual' patterns of movement that may warn of catastrophic collapse.

Future research of pre-catastrophic failure landslide-motion detection should focus on the synergy between satellite InSAR data and satellite optical images, to complement the drawbacks of each method (FIG. 6). Different inventories of slow-moving landslides at regional scales have already been created from both optical and InSAR satellite time series and include thousands of

slow-moving landslides worldwide[18,46,185–189]. In addition, we believe that back analysis of numerous case studies using remote-sensing data will allow for a better physical understanding of the landslide-rupture process and help improve detection of their precursory motions[12]. Precursor detection will benefit from machine-learning techniques, owing to the huge quantity of satellite data that are available.

We also hope that freely available remote-sensing data will improve landslide-monitoring efforts in less economically developed countries. Improving landslide monitoring in less economically developed countries is of particular interest, as they tend to be disproportionately impacted by landslides[1], such as those in the high mountains of the Himalayas, Philippines, East and Central Africa or in the Andes. We strongly encourage scientists to ensure that the methods developed are freely available to use and to train students from all countries.

Published online: 21 July 2020

1. Froude, M. J. & Petley, D. Global fatal landslide occurrence from 2004 to 2016. *Nat. Hazards Earth Syst. Sci.* **18**, 2161–2181 (2018).
2. Temple, P. H. & Rapp, A. Landslides in the Mgeta area, Western Uluguru mountains, Tanzania: Geomorphological effects of sudden heavy rainfall. *Geogr. Ann. Ser. A Phys. Geogr.* **54**, 157–193 (1972).
3. Keefer, D. K. Landslides caused by earthquakes. *Geol. Soc. Am. Bull.* **95**, 406–421 (1984).
4. Palmer, J. Creeping earth could hold secret to deadly landslides. *Nature* **548**, 384–386 (2017).
5. Mansour, M. F., Morgenstern, N. R. & Martin, C. D. Expected damage from displacement of slow-moving slides. *Landslides* **8**, 117–131 (2011).
6. Reid, M. E. et al. in *Debris-Flow Hazards Mitigation: Mechanics, Prediction, and Assessment* Vol. 1 (eds Rickenmann, D. & Chen, C.-L.) 155–166 (Millpress, 2003).
7. Booth, A. M. et al. Transient reactivation of a deep-seated landslide by undrained loading captured with repeat airborne and terrestrial lidar. *Geophys. Res. Lett.* **45**, 4841–4850 (2018).
8. Hendron, A. J. Jr & Patton, F. D. *The Vaiont Slide, a geotechnical analysis based on how geologic observations of the failure surface. Technical Report GL-85-5* (U.S. Army Corps of Engineers, 1985).
9. Intrieri, E. et al. The Maoxian landslide as seen from space: detecting precursors of failure with Sentinel-1 data. *Landslides* **15**, 123–133 (2018).
10. Handwerger, A. L., Huang, M.-H., Fielding, E. J., Booth, A. M. & Bürgmann, R. A shift from drought to extreme rainfall drives a stable landslide to catastrophic failure. *Sci. Rep.* **9**, 1569 (2019).
11. Federico, A. et al. Prediction of time to slope failure: a general framework. *Environ. Earth Sci.* **66**, 245–256 (2012).
12. Carlà, T. et al. Perspectives on the prediction of catastrophic slope failures from satellite InSAR. *Sci. Rep.* **9**, 14137 (2019).
13. Lacroix, P., Bièvre, G., Pathier, E., Kniess, U. & Jongmans, D. Use of Sentinel-2 images for the detection of precursory motions before landslide failures. *Remote. Sens. Environ.* **215**, 507–516 (2018).
14. Desrues, M., Lacroix, P. & Brenguier, O. Satellite pre-failure detection and in situ monitoring of the landslide of the Tunnel du Chambon, French Alps. *Geosciences* **9**, 313 (2019).
15. Wang, F. et al. Movement of the Shuping landslide in the first four years after the initial impoundment of the Three Gorges Dam Reservoir, China. *Landslides* **5**, 321–329 (2008).
16. Dille, A. et al. Causes and triggers of deep-seated hillslope instability in the tropics–Insights from a 60-year record of Ikoma landslide (DR Congo). *Geomorphology* **345**, 106835 (2019).
17. Nappo, N., Peduto, D., Mavrouli, O., van Westen, C. J. & Gullà, G. Slow-moving landslides interacting with the road network: analysis of damage using ancillary data, in situ surveys and multi-source monitoring data. *Eng. Geol.* **260**, 105244 (2019).
18. Lacroix, P., Dehecq, A. & Taipe, E. Irrigation-triggered landslides in a Peruvian desert caused by modern intensive farming. *Nat. Geosci.* **13**, 56–60 (2020).
19. Wu, S. et al. Zonation of the landslide hazards in the forereservoir region of the Three Gorges Project on the Yangtze River. *Eng. Geol.* **59**, 51–58 (2001).
20. Mackey, B. H. & Roering, J. J. Sediment yield, spatial characteristics, and the long-term evolution of active earthflows determined from airborne lidar and historical aerial photographs, Eel River, California. *Bulletin* **123**, 1560–1576 (2011).
21. Simoni, A., Ponza, A., Picotti, V., Berti, M. & Dinelli, E. Earthflow sediment production and Holocene sediment record in a large Apennine catchment. *Geomorphology* **188**, 42–53 (2013).
22. Coe, J. A., McKenna, J. P., Godt, J. W. & Baum, R. L. Basal-topographic control of stationary ponds on a continuously moving landslide. *Earth Surf. Process. Landf.* **34**, 264–279 (2009).
23. Bontemps, N., Lacroix, P., Larose, E., Jara, J. & Taipe, E. Rain and small earthquakes maintain a slow-moving landslide in a persistent critical state. *Nat. Commun.* **11**, 780 (2020).
24. Nereson, A. L. & Finnegan, N. J. Drivers of earthflow motion revealed by an 80 yr record of displacement from Oak Ridge earthflow, Diablo Range, California, USA. *Bulletin* **131**, 389–402 (2018).
25. Iverson, R. M. & Major, J. J. Rainfall, ground-water flow, and seasonal movement at Minor Creek landslide, northwestern California: physical interpretation of empirical relations. *Geol. Soc. Am. Bull.* **99**, 579–594 (1987).
26. Krzeminska, D., Bogaard, T., Malet, J.-P. & Van Beek, L. A model of hydrological and mechanical feedbacks of preferential fissure flow in a slow-moving landslide. *Hydrol. Earth Syst. Sci.* **17**, 947–959 (2013).
27. Hungr, O., Leroueil, S. & Picarelli, L. The Varnes classification of landslide types, an update. *Landslides* **11**, 167–194 (2013).
28. Galloway, W. The landslide in the Rhymney valley. *Nature* **73**, 425–426 (1906).
29. Miller, W. J. The landslide at Point Firmin, California. *Sci. Monthly* **32**, 464–469 (1931).
30. Benson, W. N. Landslides and their relation to engineering in the Dunedin district, New Zealand. *Econ. Geol.* **41**, 328–347 (1946).
31. Crandell, D. R. Movement of the Slumgullion earthflow near Lake City, Colorado. *Short Papers in the Geologic and Hydrologic Sciences* B136–B139 (1961).
32. Schulz, W. H., McKenna, J. P., Kibler, J. D. & Biavati, G. Relations between hydrology and velocity of a continuously moving landslide — evidence of pore-pressure feedback regulating landslide motion? *Landslides* **6**, 181–190 (2009).
33. Schulz, W. H., Kean, J. W. & Wang, G. Landslide movement in southwest Colorado triggered by atmospheric tides. *Nat. Geosci.* **2**, 863–866 (2009).
34. Schulz, W. H. et al. Landslide kinematics and their potential controls from hourly to decadal timescales: Insights from integrating ground-based InSAR measurements with structural maps and long-term monitoring data. *Geomorphology* **285**, 121–136 (2017).
35. Schulz, W. H., Smith, J. B., Wang, G., Jiang, Y. & Roering, J. J. Clayey landslide initiation and acceleration strongly modulated by soil swelling. *Geophys. Res. Lett.* **45**, 1888–1896 (2018).
36. Helmstetter, A. & Garambois, S. Seismic monitoring of Séchilienne rockslide (French Alps): Analysis of seismic signals and their correlation with rainfalls. *J. Geophys. Res. Earth Surf.* **115**, F03016 (2010).
37. Mainsant, G. et al. Ambient seismic noise monitoring of a clay landslide: Toward failure prediction. *J. Geophys. Res. Earth Surf.* **117**, F01030 (2012).
38. Travelletti, J., Sailhac, P., Malet, J.-P., Grandjean, G. & Ponton, J. Hydrological response of weathered clay-shale slopes: Water infiltration monitoring with time-lapse electrical resistivity tomography. *Hydrol. Process.* **26**, 2106–2119 (2012).
39. Provost, F., Hibert, C. & Malet, J.-P. Automatic classification of endogenous landslide seismicity using the Random Forest supervised classifier. *Geophys. Res. Lett.* **44**, 113–120 (2017).
40. Delacourt, C., Allemand, P., Casson, B. & Vadon, H. Velocity field of the "La Clapière" landslide measured by the correlation of aerial and QuickBird satellite images. *Geophys. Res. Lett.* **31**, L15619 (2004).
41. Hilley, G. E., Bürgmann, R., Ferretti, A., Novali, F. & Rocca, F. Dynamics of slow-moving landslides from permanent scatterer analysis. *Science* **304**, 1952–1955 (2004).
42. Booth, A. M., Lamb, M. P., Avouac, J.-P. & Delacourt, C. Landslide velocity, thickness, and rheology from remote sensing: La Clapière landslide, France. *Geophys. Res. Lett.* **40**, 4299–4304 (2013).
43. Lacroix, P., Berthier, E. & Maquerhua, E. T. Earthquake-driven acceleration of slow-moving landslides in the Colca valley, Peru, detected from Pléiades images. *Remote. Sens. Environ.* **165**, 148–158 (2015).
44. Lacroix, P., Araujo, G., Hollingsworth, J. & Taipe, E. Self entrainment motion of a slow-moving landslide inferred from Landsat-8 time-series. *J. Geophys. Res. Earth Surf.* **124**, 1201–1216 (2019).
45. Bennett, G. L. et al. Historic drought puts the brakes on earthflows in Northern California. *Geophys. Res. Lett.* **43**, 5725–5731 (2016).
46. Stumpf, A., Malet, J.-P. & Delacourt, C. Correlation of satellite image time-series for the detection and monitoring of slow-moving landslides. *Remote. Sens. Environ.* **189**, 40–55 (2017).
47. Handwerger, A. L. et al. Widespread initiation, reactivation, and acceleration of landslides in the northern California Coast Ranges due to extreme rainfall. *J. Geophys. Res. Earth Surf.* **124**, 1782–1797 (2019).
48. Hutchinson, J. & Bhandari, R. Undrained loading, a fundamental mechanism of mudflows and other mass movements. *Geotechnique* **21**, 353–358 (1971).
49. Van Asch, T. W. J., Malet, J.-P. & Bogaard, T. A. The effect of groundwater fluctuations on the velocity pattern of slow-moving landslides. *Nat. Hazards Earth Syst. Sci.* **9**, 739–749 (2009).
50. Lacroix, P., Perfettini, H., Taipe, E. & Guillier, B. Coseismic and postseismic motion of a landslide: Observations, modeling, and analogy with tectonic faults. *Geophys. Res. Lett.* **41**, 6676–6680 (2014).
51. Handwerger, A. L., Rempel, A. W., Skarbek, R. M., Roering, J. J. & Hilley, G. E. Rate-weakening friction characterizes both slow sliding and catastrophic failure of landslides. *Proc. Natl Acad. Sci. USA* **113**, 10281–10286 (2016).
52. RESIF/OMIV. French multidisciplinary observatory of versant instabilities. *RESIF - Réseau Sismologique et géodésique Français* (RESIF/OMIV, 2006).
53. Colombo, A., Lanteri, L., Ramasco, M. & Troisi, C. Systematic GIS-based landslide inventory as the first step for effective landslide-hazard management. *Landslides* **2**, 291–301 (2005).
54. Jaboyedoff, M. et al. in *Landslides Processes — from Geomorphologic Mapping to Dynamic Modeling* (eds Malet, J. P., Remaître, A. & Bogaard, T.) 131–137 (CERG Editions, 2009).
55. Malet, J.-P., Maquaire, O., Locat, J. & Remaître, A. Assessing debris flow hazards associated with slow moving landslides: methodology and numerical analyses. *Landslides* **1**, 83–90 (2004).
56. Corsini, A., Pasuto, A., Soldati, M. & Zannoni, A. Field monitoring of the Corvara landslide (Dolomites, Italy) and its relevance for hazard assessment. *Geomorphology* **66**, 149–165 (2005).
57. Bièvre, G. et al. Paleotopographic control of landslides in lacustrine deposits (Trièves plateau, French western Alps). *Geomorphology* **125**, 214–224 (2011).
58. Lebourg, T., Binet, S., Tric, E., Jomard, H. & El Bedoui, S. Geophysical survey to estimate the 3D sliding surface and the 4D evolution of the water pressure on part of a deep seated landslide. *Terra Nova* **17**, 399–406 (2005).
59. Strozzi, T. et al. Combined observations of rock mass movements using satellite SAR interferometry, differential GPS, airborne digital photogrammetry, and airborne photography interpretation. *J. Geophys. Res. Earth Surf.* **115**, F01014 (2010).

60. Meric, O. et al. Application of geophysical methods for the investigation of the large gravitational mass movement of Séchilienne, France. *Can. Geotech. J.* **42**, 1105–1115 (2005).
61. Corominas, J., Moya, J., Ledesma, A., Lloret, A. & Gili, J. A. Prediction of ground displacements and velocities from groundwater level changes at the Vallcebre landslide (Eastern Pyrenees, Spain). *Landslides* **2**, 83–96 (2005).
62. Mantovani, F., Pasuto, A., Silvano, S. & Zannoni, A. Collecting data to define future hazard scenarios of the Tessina landslide. *Int. J. Appl. Earth Obs. Geoinf.* **2**, 33–40 (2000).
63. Merriam, R. Portuguese bend landslide, Palos Verdes Hills, California. *J. Geol.* **68**, 140–153 (1960).
64. Scheingross, J. S. et al. Fault-zone controls on the spatial distribution of slow-moving landslides. *Bulletin* **125**, 473–489 (2013).
65. Roering, J. J. et al. Beyond the angle of repose: A review and synthesis of landslide processes in response to rapid uplift, Eel River, Northern California. *Geomorphology* **236**, 109–131 (2015).
66. Nereson, A. L., Davila Olivera, S. & Finnegan, N. J. Field and remote-sensing evidence for hydro-mechanical isolation of a long-lived earthflow in central California. *Geophys. Res. Lett.* **45**, 9672–9680 (2018).
67. Schulz, W. H. & Wang, G. Residual shear strength variability as a primary control on movement of landslides reactivated by earthquake-induced ground motion: Implications for coastal Oregon, U.S. *J. Geophys. Res. Earth Surf.* **119**, 1617–1635 (2014).
68. Coe, J. A. et al. Seasonal movement of the Slumgullion landslide determined from Global Positioning System surveys and field instrumentation, July 1998–March 2002. *Eng. Geol.* **68**, 67–101 (2003).
69. Zhang, X., Phillips, C. & Pearce, A. Surface movement in an earthflow complex, Raukumara Peninsula, New Zealand. *Geomorphology* **4**, 261–272 (1991).
70. Massey, C., Petley, D., McSaveney, M. & Archibald, G. Basal sliding and plastic deformation of a slow, reactivated landslide in New Zealand. *Eng. Geol.* **208**, 11–28 (2016).
71. Macfarlane, D. F. Observations and predictions of the behaviour of large, slow-moving landslides in schist, Clyde Dam reservoir, New Zealand. *Eng. Geol.* **109**, 5–15 (2009).
72. Furuya, G., Sassa, K., Hiura, H. & Fukuoka, H. Mechanism of creep movement caused by landslide activity and underground erosion in crystalline schist, Shikoku Island, southwestern Japan. *Eng. Geol.* **53**, 311–325 (1999).
73. Peyret, M. et al. Monitoring of the large slow Kahrod landslide in Alborz mountain range (Iran) by GPS and SAR interferometry. *Eng. Geol.* **100**, 131–141 (2008).
74. Iverson, R. M. A constitutive equation for mass-movement behavior. *J. Geol.* **93**, 143–160 (1985).
75. Malet, J.-P. & Maquaire, O. in *Proceedings of 1st International Conference on Fast Slope Movements* (eds Malet, J.-P., Maquaire, O. & Picarelli, L.) 333–340 (Patron Editore, 2003).
76. Agliardi, F., Scuderi, M. M., Fusi, N. & Collettini, C. Slow-to-fast transition of giant creeping rockslides modulated by undrained loading in basal shear zones. *Nat. Commun.* **11**, 1352 (2020).
77. Glueer, F., Loew, S., Manconi, A. & Aaron, J. From toppling to sliding: progressive evolution of the Moosfluh Landslide, Switzerland. *J. Geophys. Res. Earth Surf.* **124**, 2899–2919 (2020).
78. El Bedoui, S., Guglielmi, Y., Lebourg, T. & Pérez, J.-L. Deep-seated failure propagation in a fractured rock slope over 10,000 years: the La Clapiere slope, the south-eastern French Alps. *Geomorphology* **105**, 232–238 (2009).
79. Le Roux, O. et al. CRE dating on the head scarp of a major landslide (Séchilienne, French Alps), age constraints on Holocene kinematics. *Earth Planet. Sci. Lett.* **280**, 236–245 (2009).
80. Guerriero, L. et al. Kinematic segmentation and velocity in earth flows: a consequence of complex basal-slip surfaces. *Procedia Earth Planet. Sci.* **16**, 146–155 (2016).
81. Zerathe, S. et al. Morphology, structure and kinematics of a rainfall controlled slow-moving Andean landslide, Peru. *Earth Surf. Process. Landf.* **41**, 1477–1493 (2016).
82. Bontemps, N., Lacroix, P. & Doin, M. Inversion of deformation fields time-series from optical images, and application to the long term kinematics of slow-moving landslides in Peru. *Remote. Sens. Environ.* **210**, 144–158 (2018).
83. Van Genuchten, P. M. & De Rijke, H. On pore water pressure variations causing slide velocities and accelerations observed in a seasonally active landslide. *Earth Surf. Process. Landf.* **14**, 577–586 (1989).
84. Handwerger, A. L., Roering, J. J. & Schmidt, D. A. Controls on the seasonal deformation of slow-moving landslides. *Earth Planet. Sci. Lett.* **377**, 239–247 (2013).
85. Malet, J.-P., Maquaire, O. & Calais, E. The use of Global Positioning System techniques for the continuous monitoring of landslides: application to the Super-Sauze earthflow (Alpes-de-Haute-Provence, France). *Geomorphology* **43**, 33–54 (2002).
86. Li, X., Zhao, C., Hölter, R., Datcheva, M. & Alimardani Lavasan, A. Modelling of a large landslide problem under water level fluctuation — model calibration and verification. *Geosciences* **9**, 89 (2019).
87. Iverson, R. M. Landslide triggering by rain infiltration. *Water Resour. Res.* **36**, 1897–1910 (2000).
88. Aleotti, P. A warning system for rainfall-induced shallow failures. *Eng. Geol.* **73**, 247–265 (2004).
89. Matsuura, S., Asano, S. & Okamoto, T. Relationship between rain and/or meltwater, pore-water pressure and displacement of a reactivated landslide. *Eng. Geol.* **101**, 49–59 (2008).
90. Bayer, B., Simoni, A., Mulas, M., Corsini, A. & Schmidt, D. Deformation responses of slow moving landslides to seasonal rainfall in the Northern Apennines, measured by InSAR. *Geomorphology* **308**, 293–306 (2018).
91. Osawa, H. et al. Seasonal transition of hydrological processes in a slow-moving landslide in a snowy region. *Hydrol. Process.* **32**, 2695–2707 (2018).
92. Zhou, C., Yin, K., Cao, Y. & Ahmed, B. Application of time series analysis and PSO–SVM model in predicting the Bazimen landslide in the Three Gorges Reservoir, china. *Eng. Geol.* **204**, 108–120 (2016).
93. Zhang, X., Phillips, C. & Marden, M. A comparison of earthflow movement mechanisms on forested and grassed slopes, Raukumara Peninsula, North Island, New Zealand. *Geomorphology* **6**, 175–187 (1993).
94. Terzaghi, K. *Theoretical Soil Mechanics* (Wiley, 1943).
95. Keefer, D. K. & Johnson, A. M. *Earth flows; morphology, mobilization, and movement. Professional Paper 1264* (U.S. Government Publishing Office, 1983).
96. Picarelli, L., Urciuoli, G., Ramondini, M. & Comegna, L. Main features of mudslides in tectonised highly fissured clay shales. *Landslides* **2**, 15–30 (2005).
97. Fiolleau, S. et al. Seismic characterization of a clay-block rupture in Harmalière landslide, French Western Alps. *Geophys. J. Int.* **221**, 1777–1788 (2020).
98. Lu, N. & Godt, J. Infinite slope stability under steady unsaturated seepage conditions. *Water Resour. Res.* **44**, W11404 (2008).
99. Lu, N. & Godt, J. W. *Hillslope Hydrology and Stability* (Cambridge Univ. Press, 2013).
100. Iverson, R. M. et al. Acute sensitivity of landslide rates to initial soil porosity. *Science* **290**, 513–516 (2000).
101. Van Asch, T. W. J., Hendriks, M. R., Hessel, R. & Rappange, F. E. Hydrological triggering conditions of landslides in varved clays in the French Alps. *Eng. Geol.* **42**, 239–251 (1996).
102. Van Asch, T. J. W., Buma, J. & Van Beek, L. P. H. A view on some hydrological triggering systems in landslides. *Geomorphology* **30**, 25–32 (1999).
103. Hu, X. et al. Mobility, thickness, and hydraulic diffusivity of the slow-moving Monroe landslide in California revealed by L-band satellite radar interferometry. *J. Geophys. Res. Solid. Earth* **124**, 7504–7518 (2019).
104. Bièvre, G., Jongmans, D., Winiarski, T. & Zumbo, V. Application of geophysical measurements for assessing the role of fissures in water infiltration within a clay landslide (Trièves area, French Alps). *Hydrol. Process.* **26**, 2128–2142 (2012).
105. Krzeminska, D. M., Bogaard, T. A., van Asch, T. W. J. & van Beek, L. P. H. A conceptual model of the hydrological influence of fissures on landslide activity. *Hydrol. Earth Syst. Sci.* **16**, 1561–1576 (2012).
106. Bièvre, G. et al. Influence of environmental parameters on the seismic velocity changes in a clayey mudflow (Pont-Bourquin Landslide, Switzerland). *Eng. Geol.* **245**, 248–257 (2018).
107. Helmstetter, A. et al. Slider block friction model for landslides: Application to Vaiont and La Clapiere landslides. *J. Geophys. Res. Solid Earth* **109**, B02409 (2004).
108. Du, J., Yin, K. & Lacasse, S. Displacement prediction in colluvial landslides, Three Gorges Reservoir, China. *Landslides* **10**, 203–218 (2013).
109. Miao, H., Wang, G., Yin, K., Kamai, T. & Li, Y. Mechanism of the slow-moving landslides in Jurassic red-strata in the Three Gorges Reservoir, China. *Eng. Geol.* **171**, 59–69 (2014).
110. Tofani, V., Dapporto, S., Vannocci, P. & Casagli, N. Infiltration, seepage and slope instability mechanisms during the 20–21 November 2000 rainstorm in Tuscany, central Italy. *Nat. Hazards Earth Syst. Sci.* **6**, 1025–1033 (2006).
111. Keqiang, H., Xiangran, L., Xueqing, Y. & Dong, G. The landslides in the Three Gorges Reservoir Region, China and the effects of water storage and rain on their stability. *Environ. Geol.* **55**, 55–63 (2008).
112. Hu, X., Lu, Z., Pierson, T. C., Kramer, R. & George, D. L. Combining InSAR and GPS to determine transient movement and thickness of a seasonally active low-gradient translational landslide. *Geophys. Res. Lett.* **45**, 1453–1462 (2018).
113. Bièvre, G., Joseph, A. & Bertrand, C. Preferential water infiltration path in a slow-moving clayey earthslide evidenced by cross-correlation of hydrometeorological time series (Charlaix landslide, French Western Alps). *Geofluids* **2018**, 9593267 (2018).
Special issue "The Role and Impact of Geofluids in Geohazards".
114. Keefer, D. K. et al. Real-time landslide warning during heavy rainfall. *Science* **238**, 921–925 (1987).
115. Krøgli, I. K. et al. The Norwegian forecasting and warning service for rainfall- and snowmelt-induced landslides. *Nat. Hazards Earth Syst. Sci.* **18**, 1427–1450 (2018).
116. Berti, M. & Simoni, A. Observation and analysis of near-surface pore-pressure measurements in clay-shales slopes. *Hydrol. Process.* **26**, 2187–2205 (2012).
117. Preuth, T., Glade, T. & Demoulin, A. Stability analysis of a human-influenced landslide in eastern Belgium. *Geomorphology* **120**, 38–47 (2010).
118. Calabro, M. D., Schmidt, D. A. & Roering, J. J. An examination of seasonal deformation at the Portuguese Bend landslide, southern California, using radar interferometry. *J. Geophys. Res. Earth Surf.* **115**, F02020 (2010).
119. Helle, T. E., Nordal, S., Aagaard, P. & Lied, O. K. Long-term effect of potassium chloride treatment on improving the soil behavior of highly sensitive clay — Ulvensplitten, Norway. *Can. Geotech. J.* **53**, 410–422 (2016).
120. Helle, T. E., Aagaard, P. & Nordal, S. In situ improvement of highly sensitive clays by potassium chloride migration. *J. Geotech. Geoenviron. Eng.* **143**, 04017074 (2018).
121. Bardou, E., Bowen, P., Boivin, P. & Banfill, P. Impact of small amounts of swelling clays on the physical properties of debris-flow-like granular materials. Implications for the study of alpine debris flow. *Earth Surf. Process. Landf.* **32**, 698–710 (2007).
122. Torrance, J. K. in *Landslides: Types, Mechanisms and Modeling* Ch. 8 (eds Clague, J. J. & Stead, D.) 83–94 (Cambridge Univ. Press, 2012).
123. Tika, T. E., Vaughan, P. & Lemos, L. Fast shearing of pre-existing shear zones in soil. *Geotechnique* **46**, 197–233 (1996).
124. Scaringi, G., Hu, W., Xu, Q. & Huang, R. Shear-rate-dependent behavior of clayey bimaterial interfaces at landslide stress levels. *Geophys. Res. Lett.* **45**, 766–777 (2018).
125. Molinari, A. & Perfettini, H. Fundamental aspects of a new micromechanical model of rate and state friction. *J. Mech. Phys. Solids* **124**, 63–82 (2019).
126. Brodsky, E. E., Roeloffs, E., Woodcock, D., Gall, I. & Manga, M. A mechanism for sustained groundwater pressure changes induced by distant earthquakes. *J. Geophys. Res. Solid Earth* **108**, 2390 (2003).
127. Wang, C.-y & Chia, Y. Mechanism of water level changes during earthquakes: Near field versus intermediate field. *Geophys. Res. Lett.* **35**, L12402 (2008).
128. Sassa, K., Fukuoka, H., Scarascia-Mugnozza, G. & Evans, S. Earthquake-induced-landslides: distribution, motion and mechanisms. *Soils Found.* **36**, 53–64 (1996).
129. Wang, F., Sassa, K. & Wang, G. Mechanism of a long-runout landslide triggered by the August 1998 heavy rainfall in Fukushima Prefecture, Japan. *Eng. Geol.* **63**, 169–185 (2002).
130. Glueer, F., Loew, S. & Manconi, A. Paraglacial history and structure of the Moosfluh Landslide (1850–2016), Switzerland. *Geomorphology* **355**, 106677 (2020).
131. Carrière, S. et al. Rheological properties of clayey soils originating from flow-like landslides. *Landslides* **15**, 1615–1630 (2018).
132. Newmark, N. M. Effects of earthquakes on dams and embankments. *Geotechnique* **15**, 139–159 (1965).

133. Marc, O., Hovius, N., Meunier, P., Uchida, T. & Hayashi, S. Transient changes of landslide rates after earthquakes. *Geology* **43**, 883–886 (2015).
134. Durand, V. et al. On the link between external forcings and slope instabilities in the Piton de la Fournaise Summit Crater, Reunion Island. *J. Geophys. Res. Earth Surf.* **123**, 2422–2442 (2018).
135. Bovis, M. J. & Jones, P. Holocene history of earthflow mass movements in south-central British Columbia: the influence of hydroclimatic changes. *Can. J. Earth Sci.* **29**, 1746–1755 (1992).
136. Rutter, E. & Green, S. Quantifying creep behaviour of clay-bearing rocks below the critical stress state for rapid failure: Mam Tor landslide, Derbyshire, England. *J. Geol. Soc.* **168**, 359–372 (2011).
137. Riva, F., Agliardi, F., Amitrano, D. & Crosta, G. B. Damage-based time-dependent modeling of paraglacial to postglacial progressive failure of large rock slopes. *J. Geophys. Res. Earth Surf.* **123**, 124–141 (2018).
138. Moore, P. L. & Iverson, N. R. Slow episodic shear of granular materials regulated by dilatant strengthening. *Geology* **30**, 843–846 (2002).
139. Gabet, E. J. & Mudd, S. M. The mobilization of debris flows from shallow landslides. *Geomorphology* **74**, 207–218 (2006).
140. Iverson, R. M. Regulation of landslide motion by dilatancy and pore pressure feedback. *J. Geophys. Res. Earth Surf.* **110**, F02015 (2005).
141. Iverson, R. M. & George, D. L. Modelling landslide liquefaction, mobility bifurcation and the dynamics of the 2014 Oso disaster. *Géotechnique* **66**, 175–187 (2016).
142. Khaldoun, A. et al. Quick clay and landslides of clayey soils. *Phys. Rev. Lett.* **103**, 188301 (2009).
143. Voight, B. A method for prediction of volcanic eruptions. *Nature* **332**, 125–130 (1988).
144. Lacroix, P. & Amitrano, D. Long-term dynamics of rockslides and damage propagation inferred from mechanical modeling. *J. Geophys. Res. Earth Surf.* **118**, 2292–2307 (2013).
145. Viesca, R. C. & Rice, J. R. Nucleation of slip-weakening rupture instability in landslides by localized increase of pore pressure. *J. Geophys. Res. Solid. Earth* **117**, B03104 (2012).
146. Schaeffer, D. G. & Iverson, R. M. Steady and intermittent slipping in a model of landslide motion regulated by pore-pressure feedback. *SIAM J. Appl. Math.* **69**, 769–786 (2008).
147. Collins, B. D. & Reid, M. E. Enhanced landslide mobility by basal liquefaction: The 2014 State Route 530 (Oso), Washington, landslide. *GSA Bulletin* **132**, 451–476 (2020).
148. Chau, K. T. Onset of natural terrain landslides modelled by linear stability analysis of creeping slopes with a two-state variable friction law. *Int. J. Numer. Anal. Methods Geomech.* **23**, 1835–1855 (1999).
149. Dieterich, J. H. Modeling of rock friction: 1. Experimental results and constitutive equations. *J. Geophys. Res. Solid Earth* **84**, 2161–2168 (1979).
150. Rice, J. R. & Ruina, A. L. Stability of steady frictional slipping. *J. Appl. Mech.* **50**, 343–349 (1983).
151. Wang, G., Suemine, A. & Schulz, W. H. Shear-rate-dependent strength control on the dynamics of rainfall-triggered landslides, Tokushima Prefecture, Japan. *Earth Surf. Process. Landf.* **35**, 407–416 (2010).
152. Segall, P. & Rice, J. R. Dilatancy, compaction, and slip instability of a fluid-infiltrated fault. *J. Geophys. Res. Solid Earth* **100**, 22155–22171 (1995).
153. Samuelson, J., Elsworth, D. & Marone, C. Shear-induced dilatancy of fluid-saturated faults: experiment and theory. *J. Geophys. Res. Solid Earth* **114**, B12404 (2009).
154. Segall, P., Rubin, A. M., Bradley, A. M. & Rice, J. R. Dilatant strengthening as a mechanism for slow slip events. *J. Geophys. Res. Solid. Earth* **115**, B12305 (2010).
155. Fukuzono, T. A method to predict the time of slope failure caused by rainfall using the inverse number of velocity of surface displacement. *Landslides* **22**, 8–13_1 (1985).
156. Amitrano, D., Grasso, J. R. & Senfaute, G. Seismic precursory patterns before a cliff collapse and critical point phenomena. *Geophys. Res. Lett.* **32**, L08314 (2005).
157. Kilburn, C. R. & Petley, D. N. Forecasting giant, catastrophic slope collapse: lessons from Vajont, Northern Italy. *Geomorphology* **54**, 21–32 (2003).
158. Crosta, G. & Agliardi, F. Failure forecast for large rock slides by surface displacement measurements. *Can. Geotech. J.* **40**, 176–191 (2003).
159. Rose, N. D. & Hungr, O. Forecasting potential slope failure in open pit mines—contingency planning and remediation. *Int. J. Rock. Mech. Min. Sci.* **44**, 308–320 (2007).
160. Segalini, A., Valletta, A. & Carri, A. Landslide time-of-failure forecast and alert threshold assessment: a generalized criterion. *Eng. Geol.* **245**, 72–80 (2018).
161. Poli, P. Creep and slip: Seismic precursors to the Nuugaatsiaq landslide (Greenland). *Geophys. Res. Lett.* **44**, 8832–8836 (2017).
162. Bell, A. F. Predictability of landslide timing from quasi-periodic precursory earthquakes. *Geophys. Res. Lett.* **45**, 1860–1869 (2018).
163. Fan, X. et al. Failure mechanism and kinematics of the deadly June 24th 2017 Xinmo landslide, Maoxian, Sichuan, China. *Landslides* **14**, 2129–2146 (2017).
164. Skarbek, R. M., Rempel, A. W. & Schmidt, D. A. Geologic heterogeneity can produce aseismic slip transients. *Geophys. Res. Lett.* **39**, L21306 (2012).
165. Bell, A. F., Naylor, M., Heap, M. J. & Main, I. G. Forecasting volcanic eruptions and other material failure phenomena: an evaluation of the failure forecast method. *Geophys. Res. Lett.* **38**, L15304 (2011).
166. Lipovsky, B. P. & Dunham, E. M. Slow-slip events on the Whillans Ice Plain, Antarctica, described using rate-and-state friction as an ice stream sliding law. *J. Geophys. Res. Earth Surf.* **122**, 973–1003 (2017).
167. Minchew, B. M. & Meyer, C. R. Dilation of subglacial sediment governs incipient surge motion in glaciers with deformable beds. *Proc. R. Soc. A Math. Phys. Eng. Sci.* **476**, 20200033 (2020).
168. Gomberg, J., Bodin, P., Savage, W. & Jackson, M. E. Landslide faults and tectonic faults, analogs?: The Slumgullion earthflow, Colorado. *Geology* **23**, 41–44 (1995).
169. Dmitrieva, K., Hotovec-Ellis, A. J., Prejean, S. & Dunham, E. M. Frictional-faulting model for harmonic tremor before redoubt volcano eruptions. *Nat. Geosci.* **6**, 652–656 (2013).
170. Le Breton, M. et al. Passive radio-frequency identification ranging, a dense and weather-robust technique for landslide displacement monitoring. *Eng. Geol.* **250**, 1–10 (2019).
171. Madson, A., Fielding, E., Sheng, Y. & Cavanaugh, K. High-resolution spaceborne, airborne and in situ landslide kinematic measurements of the Slumgullion landslide in Southwest Colorado. *Remote. Sens.* **11**, 265 (2019).
172. Thomas, A. M., Spica, Z., Bodmer, M., Schulz, W. H. & Roering, J. J. Using a dense seismic array to determine structure and site effects of the two towers earthflow in northern California. *Seismol. Res. Lett.* **91**, 913–920 (2020).
173. Truffert, C. et al. Large 3D resistivity and IP measurement of the Séchilienne landslide using the FullWaver system. *Proc. EAGE-HAGI 1st Asia Pacfic Meeting on Near Surface Geoscience and Engineering* **2018**, 1–4 (2018).
174. Loke, M., Chambers, J., Rucker, D., Kuras, O. & Wilkinson, P. Recent developments in the direct-current geoelectrical imaging method. *J. Appl. Geophys.* **95**, 135–156 (2013).
175. Perrone, A., Lapenna, V. & Piscitelli, S. Electrical resistivity tomography technique for landslide investigation: A review. *Earth Sci. Rev.* **135**, 65–82 (2014).
176. Uhlemann, S. et al. Four-dimensional imaging of moisture dynamics during landslide reactivation. *J. Geophys. Res. Earth Surf.* **122**, 398–418 (2017).
177. Uhlemann, S. et al. Assessment of ground-based monitoring techniques applied to landslide investigations. *Geomorphology* **253**, 438–451 (2016).
178. Whiteley, J. S., Chambers, J. E., Uhlemann, S., Wilkinson, P. B. & Kendall, J. M. Geophysical monitoring of moisture-induced landslides: a review. *Rev. Geophys.* **57**, 106–145 (2019).
179. Gariano, S. L. & Guzzetti, F. Landslides in a changing climate. *Earth Sci. Rev.* **162**, 227–252 (2016).
180. Carlà, T., Farina, P., Intrieri, E., Ketizmen, H. & Casagli, N. Integration of ground-based radar and satellite InSAR data for the analysis of an unexpected slope failure in an open-pit mine. *Eng. Geol.* **235**, 39–52 (2018).
181. Dong, J. et al. Measuring precursory movements of the recent Xinmo landslide in Mao County, China with Sentinel-1 and ALOS-2 PALSAR-2 datasets. *Landslides* **15**, 135–144 (2018).
182. Roberts, N. J. et al. Changes in ground deformation prior to and following a large urban landslide in La Paz, Bolivia, revealed by advanced InSAR. *Nat. Hazards Earth Syst. Sci.* **19**, 679–696 (2019).
183. Walter, T. R. et al. Complex hazard cascade culminating in the Anak Krakatau sector collapse. *Nat. Commun.* **10**, 4339 (2019).
184. Crosta, G. B. & Agliardi, F. How to obtain alert velocity thresholds for large rockslides. *Phys. Chem. Earth Parts A/B/C* **27**, 1557–1565 (2002).
185. Bennett, G. L., Miller, S. R., Roering, J. J. & Schmidt, D. A. Landslides, threshold slopes, and the survival of relict terrain in the wake of the Mendocino Triple junction. *Geology* **44**, 363–366 (2016).
186. Handwerger, A. L., Roering, J. J., Schmidt, D. A. & Rempel, A. W. Kinematics of earthflows in the Northern California Coast Ranges using satellite interferometry. *Geomorphology* **246**, 321–333 (2015).
187. Dini, B., Manconi, A. & Loew, S. Investigation of slope instabilities in NW Bhutan as derived from systematic DInSAR analyses. *Eng. Geol.* **259**, 105111 (2019).
188. Strozzi, T. et al. Satellite SAR interferometry for the improved assessment of the state of activity of landslides: A case study from the Cordilleras of Peru. *Remote. Sens. Environ.* **217**, 111–125 (2018).
189. Pham, M. Q., Lacroix, P. & Doin, M. P. Sparsity optimization method for slow-moving landslides detection in satellite image time-series. *IEEE Trans. Geosci. Remote Sens.* **57**, 2133–2144 (2018).
190. Roering, J. J., Stimely, L. L., Mackey, B. H. & Schmidt, D. A. Using DInSAR, airborne LiDAR, and archival air photos to quantify landsliding and sediment transport. *Geophys. Res. Lett.* **36**, L19402 (2009).
191. Kelsey, H. M. Earthflows in Franciscan melange, Van Duzen River basin, California. *Geology* **6**, 361–364 (1978).
192. Finnegan, N. J. et al. River channel width controls blocking by slow-moving landslides in California's Franciscan mélange. *Earth Surf. Dyn.* **7**, 879–894 (2019).
193. Delbridge, B. G., Bürgmann, R., Fielding, E., Hensley, S. & Schulz, W. H. Three-dimensional surface deformation derived from airborne interferometric UAVSAR: application to the Slumgullion Landslide. *J. Geophys. Res. Solid Earth* **121**, 3951–3977 (2016).
194. Stumpf, A., Malet, J. P., Allemand, P. & Ulrich, P. Surface reconstruction and landslide displacement measurements with Pléiades satellite images. *ISPRS J. Photogramm. Remote Sens.* **95**, 1–12 (2014).
195. Schlögel, R. et al. Multi-temporal X-band radar interferometry using corner reflectors: Application and validation at the Corvara Landslide (Dolomites, Italy). *Remote Sens.* **9**, 739 (2017).
196. Chambers, J. et al. Three-dimensional geophysical anatomy of an active landslide in Lias Group mudrocks, Cleveland Basin, UK. *Geomorphology* **125**, 472–484 (2011).
197. Petley, D., Mantovani, F., Bulmer, M. & Zannoni, A. The use of surface monitoring data for the interpretation of landslide movement patterns. *Geomorphology* **66**, 133–147 (2005).
198. Massey, C. I., Petley, D. N. & McSaveney, M. Patterns of movement in reactivated landslides. *Eng. Geol.* **159**, 1–19 (2013).
199. Baum, R. L., Messerich, J. & Fleming, R. W. Surface deformation as a guide to kinematics and three-dimensional shape of slow-moving, clay-rich landslides, Honolulu, Hawaii. *Environ. Eng. Geosci.* **4**, 283–306 (1998).
200. O'Brien, G. A., Cox, S. C. & Townend, J. Spatially and temporally systematic hydrologic changes within large geoengineered landslides, Cromwell Gorge, New Zealand, induced by multiple regional earthquakes. *J. Geophys. Res. Solid Earth* **121**, 8750–8773 (2016).
201. Casson, B., Delacourt, C., Baratoux, D. & Allemand, P. Seventeen years of the "La Clapiere" landslide evolution analysed from ortho-rectified aerial photographs. *Eng. Geol.* **68**, 123–139 (2003).
202. Warrick, J. A., Ritchie, A. C., Schmidt, K. M., Reid, M. E. & Logan, J. Characterizing the catastrophic 2017 Mud Creek landslide, California, using repeat structure-from-motion (SfM) photogrammetry. *Landslides* **16**, 1201–1219 (2019).
203. Sassa, K. The movement and the mechanism of a crystalline schist landslide "Zentoku" in Japan. *Proc. Interpraevent 1980* **1**, 85–106 (1980).

204. Oppikofer, T., Jaboyedoff, M., Blikra, L., Derron, M.-H. & Metzger, R. Characterization and monitoring of the Åknes rockslide using terrestrial laser scanning. *Nat. Hazards Earth Syst. Sci.* **9**, 1003–1019 (2009).
205. Grøneng, G., Christiansen, H. H., Nilsen, B. & Blikra, L. H. Meteorological effects on seasonal displacements of the Åknes rockslide, western Norway. *Landslides* **8**, 1–15 (2011).
206. Ganerød, G. V. et al. Geological model of the Åknes rockslide, western Norway. *Eng. Geol.* **102**, 1–18 (2008).
207. Kos, A. et al. Contemporary glacier retreat triggers a rapid landslide response, Great Aletsch Glacier, Switzerland. *Geophys. Res. Lett.* **43**, 12,466–12,474 (2016).
208. Cappa, F., Guglielmi, Y., Viseur, S. & Garambois, S. Deep fluids can facilitate rupture of slow-moving giant landslides as a result of stress transfer and frictional weakening. *Geophys. Res. Lett.* **41**, 61–66 (2014).
209. Lacroix, P. & Helmstetter, A. Location of seismic signals associated with microearthquakes and rockfalls on the Séchilienne landslide, French Alps. *Bull. Seismol. Soc. Am.* **101**, 341–353 (2011).
210. Marone, C. Laboratory-derived friction laws and their application to seismic faulting. *Annu. Rev. Earth Planet Sci.* **26**, 643–696 (1998).

Acknowledgements
Part of this research was carried out at the Jet Propulsion Laboratory, California Institute of Technology, under a contract with the National Aeronautics and Space Administration (NASA). P.L. and G.B. are part of LabEx OSUG@2020 (ANR10 LABX56).

Author contributions
All authors contributed to all aspects of the article.

Competing interests
The authors declare no competing interests.

Peer review information
Nature Reviews Earth & Environment thanks E. Intrieri, X. Hu and F. Zhang for their contribution to the peer review of this work.

RELATED LINKS
USGS-USA: https://www.usgs.gov/natural-hazards/landslide-hazards/monitoring